Signatures of Hydrodynamic Transport in an Electron System

by

Haoyu Guo

Submitted to the Department of Physics
in partial fulfillment of the requirements for the degree of

BACHELOR OF SCIENCE

at the

MASSACHUSETTS INSTITUTE OF TECHNOLOGY

June 2018

Signature redacted

Author .....
Department of Physics
May 11, 2018

Signature redacted

Certified by .....
Leonid S. Levitov
Professor, Department of Physics
Thesis Supervisor

Signature redacted

Accepted by .....
Scott Hughes
Professor, Interim Physics Associate Head, Department of Physics

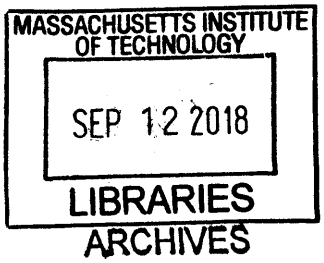

Signatures of Hydrodynamic Transport in an Electron System

by

Haoyu Guo

Submitted to the Department of Physics
on May 11, 2018, in partial fulfillment of the
requirements for the degree of
BACHELOR OF SCIENCE

Abstract

Electrons in strongly-correlated systems move in a neatly coordinated manner, in many ways resembling the movement of viscous fluids and leading to surprising collective behaviors. Here we explore how the hydrodynamic behavior manifests itself in the electron transport through nanoscale constrictions. Free electron flows through constrictions in metals are often regarded as an ultimate high-conduction charge transfer mechanism. However, as shown in this thesis, interactions can facilitate transport and give rise to superballistic conduction, allowing conductance to exceed the ballistic limit value. In other words, interactions and viscous effects, rather than presenting a hindrance for conduction, help increase carrier mobility and suppress dissipation. This interesting behavior represents a clear signature of the electron hydrodynamic regime, and provides a way to determine electron viscosity. These results show that interactions and viscous effects can facilitate high-mobility transport, granting a new route for designing low-power nanoscale devices.

Thesis Supervisor: Leonid S. Levitov
Title: Professor, Department of Physics

Acknowledgments

First of all, I would like to thank my research and thesis supervisor, Prof. Leonid Levitov. I have been working with Prof. Levitov since my sophomore year, and he has always been a great mentor. From him, I not only learned interesting physics but also got to know how to do research and how to present it. During the time working with Prof. Levitov, I developed and solidified my interest in theoretical condensed matter physics, and finally decided to pursue a doctoral degree in this direction at Harvard.

I would also like to thank my research collaborators. I benefited from the weekly discussions with Patrick Ledwith, who contributed a lot of insights to our research. I also learned a lot about fluid dynamics from Prof. Gregory Falkovich and Dr. Ekin Ilseven.

It has been a great pleasure to spend three years at MIT in the physics and the math department. My thank goes to the professors who have taught me interesting physics. I would like to thank Prof. Hong Liu, for his wonderful QFT and string theory classes and a summer project in field theory; Prof. Washington Taylor, for the topics in QFT, string theory, and geometry; and Prof. Jesse Thaler, Prof. Senthil Todadri, Prof. Mehran Kardar, Prof. Gunther Roland, Prof. William Detmold, Prof. Tracy Slatyer, Prof. Alan Guth, Prof. Aram Harrow, Prof. Robert Jaffe, Prof. Martin Zwierlein. I would also like to thank Cyuan-han, who has gone through so many physics and math classes with me together, including JLab; Hengyun(Harry), who has offered me lots of advice on physics career and graduate school application; Yibo, Yijun, Jingwen, Jingpin, Zijin, Chenxing(Tony), Deng, for the wonderful time we had at Baker House.

Finally, I want to thank my family, especially my parents, for all the love and support that they have provided for me.

Contents

List of Figures

List of Tables

Chapter 1

Introduction

Hydrodynamics, broadly defined, is an approach that uses symmetries and conservation laws to describe systems of many strongly-interacting particles [8, 36]. It starts with a microscopic picture on microscales and connects it to the hydrodynamic fields on macroscales. These fields are defined as the densities associated with the globally conserved quantities such as particle densitiy, total momentum density, and the energy density. The micro/macro connection, provided by the kinetic theory, serves as a natural framework to understand how an orderly collective behavior at large lengthscales arises from chaotic dynamics at microscopic lengthscales.

The idea that the macroscopic behavior of fluids can be explained by microscopic collisions between atoms goes back to the age of Maxwell and Boltzmann. It links the hydrodynamic variables to the fundamental conservation laws and symmetries of space-time, and helps to tackle the hard questions about the arrow of time, entropy, and the relation between chaos and determinism. But the kinetic theory and hydrodynamics are not merely deep and powerful, they are also tremendously useful, as they provide solid foundations to fluid mechanics and gas dynamics.

Recently there has been a lot of interest in extending the ideas of hydrodynamics beyond the traditional domain of classical fluids. In the last decade they were successfully applied to explore the collective behaviors of strongly-interacting particles in different areas of physics. Diverse systems of current interest fall into that framework, ranging from ultracold atomic gases ($T \sim 10^{-6}$K) to ultrahot quark-gluon plasmas

generated in heavy-ion colliders ($T \sim 10^{12}$K). Other examples include strongly-interacting matter described by string theory, as well as electron fluids in strange metals—a condensed matter system which is believed to hold key to understanding the high-temperature superconductivity. Quite remarkably, due to the conservation laws originating from fundamental symmetries of space-time, all these systems share the common long-wavelength behavior resembling viscous fluids.

Here we discuss recent progress in applying the ideas of hydrodynamics to electron systems in solids. Usually electrons in solids move as ball bearings in a pinball machine, losing their energy and momentum due to collisions with disorder and phonons. A different situation arises when strong electron-electron (ee) interactions lead to rapid *elastic* collisions [7, 9, 8, 10]. While electrons lose their identity nearly instantly in such collisions, the net energy and momentum remain conserved. Rather than being dissipated, the momenta and energies of the particles are quickly passed from one particle to another, taking on a new role of collective variables. As a result, the system is truly chaotic on a microscale but at larger lengthscales obeys conservation laws resembling those in classical hydrodynamics.

The notion of an electron system behaving as a viscous fluid may seem paradoxical. And yet, as discussed below, it proved to be quite useful for understanding electronic properties of high-mobility electron systems, in particular graphene [24, 25, 26, 27]. An atomically thin carbon monolayer discovered a decade ago, graphene has become a benchmark system for modern nanoscience. One attractive aspect of graphene is that it provides many sought-after qualities of an electron fluid. This is so because electrons in this material behave as relativistic particles coupled by long-range forces that are pretty strong, whereas the effects due to disorder and electron-phonon scattering are relatively weak. With a possible exception of exotic fluids such as quark-gluon plasmas, graphene may be closer to the notion of a perfect strongly interacting fluid than any other system we know.

But while that's true in theory, the question is, even if we have this fluid-like behavior, how do we detect it? Unlike ordinary fluids, where you can directly track the flow by putting some beads in it, for example, here we don't have a way to view

it directly. This is the question that will be addressed in this thesis.

As we will show, there are distinct signatures of hydrodynamic behavior of an electron system directly accessible by routine transport measurements. In a nutshell, viscous electron fluids can flow more easily than electron gases, with lower resistance and smaller dissipation. The tendency of electron collisions to suppress electric resistance and create low-loss viscous flows is not just surprising, it seemingly goes against traditional theory. However, even though it may seem counterintuitive, very soon after the effect was predicted [34] it was verified in transport measurements [35]. So now we have a very distinctive behavior that can serve as a litmus test of electron hydrodynamics.

This thesis is based on a previous publication by the author [34].

1.1 Summary of the main results

The reason why electron-electron (ee) interactions enhance conduction can be understood intuitively for transport through a slit (or, constriction) pictured in Fig. 1-1. In both the ballistic and the hydrodynamic regimes, the dissipation of momentum only happens at the boundary of the system. However, in the ballistic case the phase space for electron transmission is more restricted than in the hydrodynamic case. Indeed, as shown in Fig. 1-1, a ballistic electron can only passes through the slit if its initial velocity points in the directions towards the slit. Crucially, this phase space constraint is lifted in the hydrodynamic regime. In this case, because of frequent ee collisions, electrons travel over zig-zag paths with a relatively short step. Because of frequent ee scattering, the trajectory of a electron is not mandated by its initial velocity, and consequently electrons all over the phase space have non-zero probability to go through the slit.

This argument, which suggests that conduction in the hydrodynamic regime is enhanced compared to the ballistic regime, can be restated in terms of dissipation. The travel time from a given point inside the system to the boundary, where momentum is eventually dissipated, is longer for zig-zag paths than for straight paths.

Consequently the probability for a given electron in the bulk to hit the boundary and dissipate momentum is lower than that in the ballistic regime. This probability decreases as the ee scattering rate increases. Low dissipation rate translates into lower resistance and higher conductance.

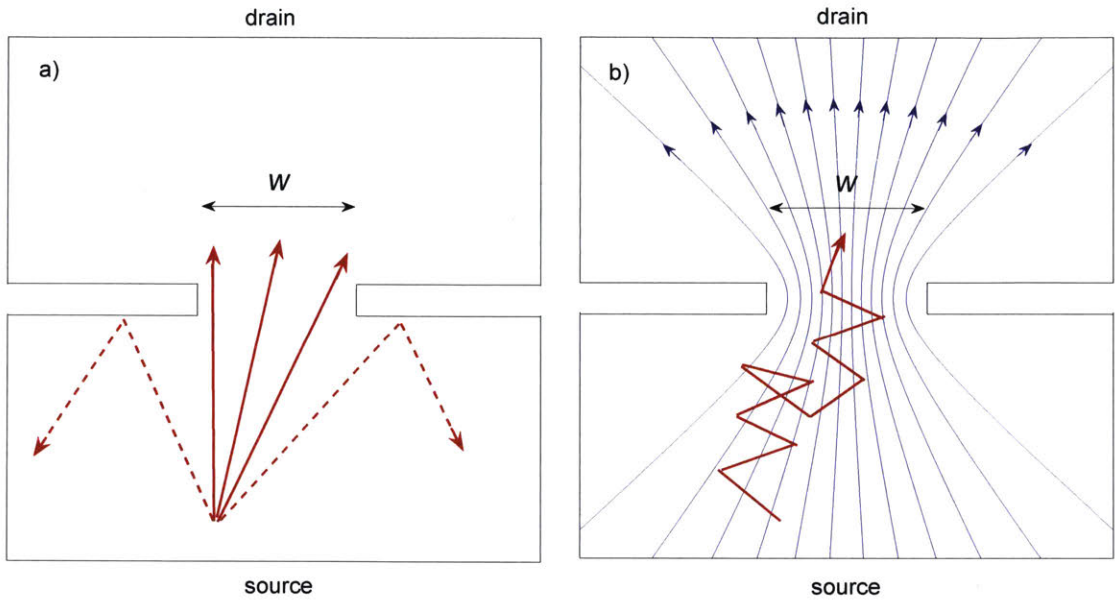

Figure 1-1: The difference between ballistic transport and hydrodynamic transport. (a) In the ballistic regime, electrons travel in straight trajectories and only few can pass through the slit. (b) In the hydrodynamic regime, electrons travel in zig-zag paths and most of them can pass through the slit.

The intuitive picture described above indicates that hydrodynamic flows use the phase space more efficiently than ballistic flows do, and this difference must be reflected in the conductance of the system. On a quantitative level, the difference between the two regimes can be understood by considering the extreme hydrodynamic regime $l_{ee} \ll w$, where l_{ee} is the electron mean free path in the bulk and w is the slit width. In this case, as we will show below, conductance can be expressed through the electron viscosity

$$G_{\text{vis}}(w) = \frac{\pi n^2 e^2 w^2}{32\eta}, \quad w \gg l_{\text{ee}}, \tag{1.1}$$

where n and e are the carrier density and charge. The viscosity $\eta \propto l_{ee}$ goes inversely

with the strength of ee interaction[1].

In the opposite limit, $l_{\rm ee} \gg w$, the ballistic free-fermion model [2, 6] predicts the conductance value (see below)

$$G_{\rm ball}(w) = \frac{2e^2}{h} N, \quad N = 2w/\lambda_F, \tag{1.2}$$

where $N \approx 2w/\lambda_F$ is the number of open transmission channels. The conductance $G_{\rm vis}$ grows with width faster than $G_{\rm ball}$. Therefore, for large enough w, viscous transport yields conductance values in excess the ballistic values. Quantitatively, at $w \gg l_{ee}$, the viscous conductance value behaves as $G_{\rm vis} \propto G_{\rm ball} \frac{w}{l_{ee}}$ (see below). The factor w/l_{ee} describes the effect of conductance enhancement due to ee collisions.

Luckily, the unique properties of graphene allow to simultaneously explore different transport regimes, the collisionless ballistic regime, the ee-collision dominated hydrodynamic regime and the ohmic regime. Indeed, in the low-temperature limit the ee scattering is suppressed by fermion exclusion whereas phonons are not thermally excited. As a result the system is found in the ballistic regime. At elevated temperature T, the ee scattering rate grows as T^2 while the electron-phonon scattering rate grows as T [37], so the ee scattering is dominant and the system enters the hydrodynamic regime. At even higher temperatures the electron-phonon scattering wins over the ee scattering, giving rise to a conventional ohmic behavior. Therefore these different regimes can be made experimentally accessible in a single graphene device, in which by adjusting temperature and electron density one can move freely between different regimes.

Below we present a detailed theory of the crossover between these regimes, focusing on transport through a slit in the geometry of Fig.1-1. In chapter 2 we review the basics of ballistic transport theory and introduce the hydrodynamic description of the electron system. In chapter 3, which is the central part of this thesis, we introduce a Boltzmannesque approach that allows to tackle the problem of the crossover between

[1]We note that the proportionality relation $\eta \propto l_{ee}$ is somewhat counterintuitive and often leads to confusion. Indeed, stronger ee interactions imply a shorter mean free path and hence a smaller viscosity, so a more viscous fluid has smaller viscosity than a less viscous fluid!

these regimes. Starting from the Boltzmann equation for particles moving in the slit geometry, we formulate an approach that transforms the integral-differential Boltzmann equation in a four-dimensional phase space $(\mathbf{r}, \mathbf{p})$ into a simple one-dimensional integral equation on the slit line. By solving this equation we determine the potential distribution induced by a current flowing through the slit and use it to evaluate conductance. The conductance at the crossover is found to be given by a simple addition rule

$$G = G_{\text{ball}} + G_{\text{hydro}}, \tag{1.3}$$

where the two terms, G_{ball} and G_{hydro}, are the ballistic and hydrodynamic contributions to conductance introduced above (Eqs.(1.1),(1.2)). Added together, they describe conductance across the ballistic-to-viscous crossover.

Chapter 2

Ballistic and Hydrodynamic Transport Through a Slit.

2.1 Free-Fermion Transport

In a degenerate Fermi gas particle collisions are blocked by fermion exclusion. As a result, at low temperatures electrons exhibit *ballistic free-particle behavior,* moving along straight trajectories and occasionally changing direction due to disorder or phonon scattering [2, 3, 4, 5, 6]. In this regime, the free electron system achieves its highest conduction capability known as the Landauer ballistic limit. Theory of ballistic conductance was first developed for transport in three-dimensional metals by Landauer and, independently, by Sharvin who also performed some experiments [1, 2]. Theory of ballistic conduction was thoroughly tested in two-dimensional electron gases after constrictions with gate-tunable width have become available in split-gate devices. By transport measurements, van Wees et al [3] and Wharam et al [4] have shown that conductance of these constrictions increases in e^2/h-quantized steps as a function of the constriction width. The observation of conductance quantization came as a surprise and it took some effort to understand its relation to Landauer's and Sharvin's work. In this chapter, we summarize the key aspects of ballistic transport and derive the ballistic conductance for a 2D slit geometry pictured in Fig. 2-1. This will set the stage for the next section where we consider the effects of ee collisions.

As a disclaimer, in this thesis we will not be concerned with the effects of conductance quantization, adopting the quasiclassical approach of Ref.[2] which treats the transport problem as classical dynamics of degenerate fermions. Such an approach is valid when the constriction width and other relevant system dimensions are much greater than the electron wavelength, $w \gg \lambda_F$. The interplay between the quantized ballistic transport and electron collisions is a fascinating topic that will be a subject of future work.

Conductance in the ballistic limit can be linked to the flux of particles through the constriction induced by a voltage bias. We model the constriction as a slit of width w as shown in Fig.2-1. Electrons pass freely through the slit and are backreflected outside the opening. To derive the conductance, we assume that the reservoirs above and below the slit supply equilibrium particle distributions with the chemical potentials $\mu_S = \mu + eV/2$ (source) and $\mu_D = \mu - eV/2$ (drain) respectively, where e is electron charge and $V \ll \mu/e$ is the voltage bias across the slit. We first carry out the analysis treating electrons as free fermions, and then discuss the validity of this approximation and improve on it by introducing a simple approach that helps to understand the role of interactions.

Now, let us consider electrons that pass through the slit. Since there is no scattering at all, the occupation numbers of the corresponding electronic states are determined by the chemical potentials in reservoirs, as shown in Fig.2-1. In particular, at any point within the slit, $-w/2 < x < w/2$, $y = 0$, the momentum distribution is an equal mixture of the distributions supplied by the source and drain:

$$n_k = \begin{cases} f(\varepsilon_k - \mu_S), & k_y > 0; \\ f(\varepsilon_k - \mu_D), & k_y < 0; \end{cases}, \qquad \mu_{S(D)} = \mu \pm eV/2, \tag{2.1}$$

where $f(\varepsilon_k - \mu) = 1/(e^{\beta(\varepsilon_k - \mu)} + 1)$ is the equilibrium Fermi distribution. Below we assume, for simplicity, a parabolic dispersion relation $\varepsilon_k = \hbar^2 k^2/2m$. Transport of particles with nonparabolic dispersion can be handled using the effective mass approximation. At $y = 0$, there is no current outside the slit, whereas inside the slit

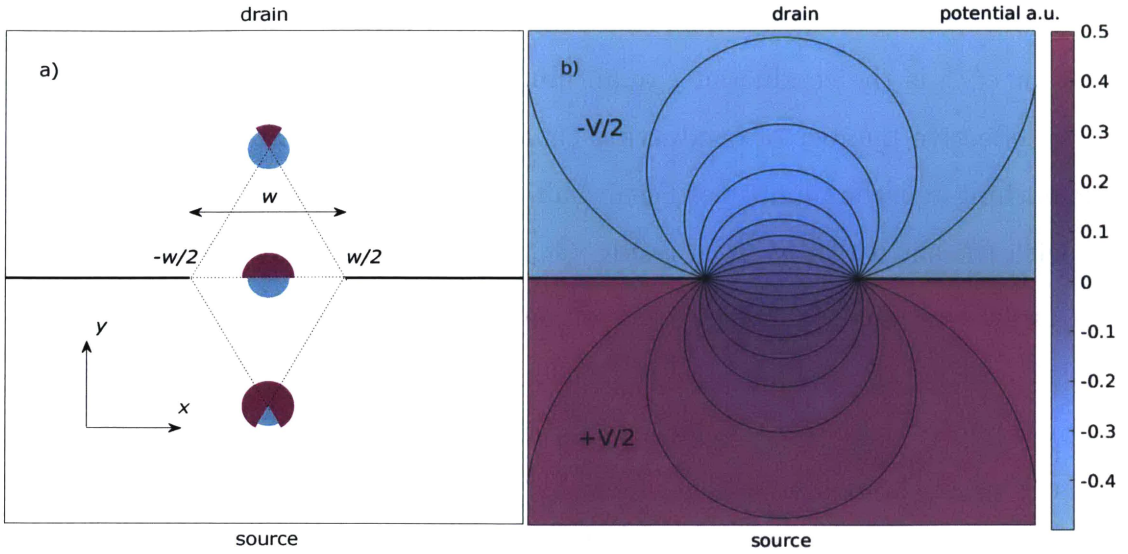

Figure 2-1: Ballistic free-fermion transport through a slit of width w positioned at $y = 0$, which connects two reservoirs extending indefinitely up and down. a) The reservoirs emit free-fermion distributions $|\mathbf{p}| < p_F^{(S)}$, $|\mathbf{p}| < p_F^{(D)}$. The Fermi momenta are unequal, $p_F^{(S)} \neq p_F^{(D)}$, when a potential bias is applied between the reservoirs, $eV = \mu_S - \mu_D$. The distributions mix due to particles moving through the slit, giving rise to structured position-dependent momentum distributions looking like a sliced pie. This is shown schematically with two colors representing particles from the two reservoirs. The $\mathbf{p}/-\mathbf{p}$ asymmetry of the distributions translates into a nonzero current density. b) The potential distribution due to current through the slit. Potential is calculated from the total particle density in the momentum distributions pictured in panel (a) by accounting for charge neutrality (see text). The resulting potential at a given point is proportional to the angle at which the slit is seen from that point, which is equal to the angular size of the pie slices in (a). The contours of constant potential therefore represent the arcs of circles that share the slit as a common chord.

the x-independent distribution in Eq.(2.1) gives a uniform current density:

$$j_y = ge \int \frac{\mathrm{d}^2 k}{(2\pi)^2} n_k v_y = N \frac{ge^2 V}{h}, \tag{2.2}$$

where $h = 2\pi\hbar$ is Planck's constant, $\lambda_F = \frac{h}{\sqrt{2m\mu}}$ is the Fermi wavelength, $N = 2w/\lambda_F$ is the effective number of transmission channels, Eq.(1.2), and the integer factor g accounts for spin and valley degeneracy. The value g depends on the system bandstructure (e.g. $g = 2$ for GaAs and $g = 4$ for graphene). Taking the ratio of the current and the voltage bias we obtain the conductance value

$$G_{\text{ball}} = g \frac{e^2}{h} \frac{2w}{\lambda_F}. \tag{2.3}$$

Eq.(2.3) is the seminal Landauer-Sharvin result for ballistic conductance. The dimensional factor e^2/h is the conductance quantum, and the dimensionless factor $2w/\lambda_F$ counts the effective number of conducting channels in the slit. The latter quantity, which is nothing but the number of Fermi half-wavelengths that fit in the slit, scales linearly with the slit width w. As a result, G_{ball} also scales linearly with w.

It is interesting that, although electron motion through the slit is completely unimpeded, so that no dissipation of their energy and momentum occurs within the slit, it gives rise to a finite resistance. This may seem paradoxical and begs a few questions. One is about dissipation which, by virtue of Ohm's law, is an inevitable attribute of finite resistance. Sure enough, ballistic transport also leads to dissipation. However, while potential induced by current drops near the slit (see Fig.2-1 and discussion below), the dissipation takes place far away from the slit in the reservoirs. The potential drop across the slit therefore does not reflect the locality of dissipation (which does not take place within the slit). Instead, the potential drop originates from space charge buildup due to the particles that undergo backscattering, as shown in Fig.1-1. The backscattered particles which do not make it through the constriction can also be viewed as the main cause of finite resistance. This is seen most easily by considering the situation when nearly all incident particles pass, described by the limit of a wide constriction $2w/\lambda_F \to \infty$. In this case, indeed, the conductance diverges and resistance vanishes.

We also note that in the quantum problem, in which transmission through the slit is treated as quantum-mechanical scattering, the number of conducting modes $2w/\lambda_F$ is an integer. One can therefore expect that the dependence of conductance on w will exhibit quantum oscillations with period $\Delta w = \lambda_F/2$. Such oscillations are indeed observed as a correction to the linear dependence in Eq.(2.3) of the form of periodic staircase with e^2/h-quantized step height[3, 4].

Next we discuss the effect of interactions and derive the potential distribution induced by current flowing through the slit. This is done most easily by employing the condition of quasineutrality, i.e. an apparent overall neutrality arising due to long-range interactions suppressing density fluctuations at large lengthscales. Classical

dynamics of momentum distribution $n(\mathbf{p}, \mathbf{r}, t)$ can be written as Liouville evolution

$$\partial_t n + \{n, H\} = 0, \quad H = \frac{\mathbf{p}^2}{2m} + eU(\mathbf{r}), \tag{2.4}$$

where $U(\mathbf{r})$ is the potential of current-induced space charge and $\{...\}$ are Poisson brackets. Explicit calculation gives collisionless Liouville-Boltzmann equation

$$\partial_t n + \mathbf{v}\nabla_{\mathbf{r}} n + e\mathbf{E}\nabla_{\mathbf{p}} n = 0, \quad \mathbf{E} = -\nabla U, \tag{2.5}$$

which must be solved together with the boundary conditions posed at the $y = 0$ boundary outside the slit.

A solution of this problem that matches the asymptotic values in reservoirs can be found by solving first-order differential equation in Eq.(2.5) by the method of characteristics. The result is a structured distribution of the form resembling a sliced pie, of the form illustrated in Fig.2-1 (a):

$$n(\mathbf{p}, \mathbf{r}) = t_S(\mathbf{p}, \mathbf{r}) f(\varepsilon_k - \mu_S + eU(\mathbf{r})) + t_D(\mathbf{p}, \mathbf{r}) f(\varepsilon_k - \mu_D + eU(\mathbf{r})). \tag{2.6}$$

The probabilities $t_{S(D)}(\mathbf{p}, \mathbf{r})$ describe accessibility of a particular point of phase space from a given reservoir:

$$t_S(\mathbf{p}, \mathbf{r}) = \begin{cases} 1, & \theta_1(\mathbf{r}) < \theta_p < \theta_2(\mathbf{r}) \\ 0, & \text{else} \end{cases}, \qquad t_D(\mathbf{p}, \mathbf{r}) = 1 - t_S(\mathbf{p}, \mathbf{r}). \tag{2.7}$$

Here θ_p is the electron momentum azimuthal angle and the condition $\theta_1(\mathbf{r}) < \theta_p < \theta_2(\mathbf{r})$ specifies momenta of particles arriving at a point $\mathbf{r}$ from the first reservoir. The values $\theta_{1,2}(\mathbf{r})$ are

$$\begin{aligned} \theta_1(\mathbf{r}) &= \arg\left(x - \frac{w}{2} + iy\right) = \arctan\frac{y}{x - \frac{w}{2}}, \\ \theta_2(\mathbf{r}) &= \arg\left(x + \frac{w}{2} + iy\right) = \arctan\frac{y}{x + \frac{w}{2}}, \end{aligned} \tag{2.8}$$

where we use the branch of arctan that does not have π-jumps, giving an expression without discontinuities at $x = \pm w/2$. This corresponds to the angles that the dotted lines in Fig.2-1 (a) make with the x axis.

The solution in Eq.(2.6) is obtained assuming that particles move freely along straight paths, ignoring the deflection of particle velocities due to the field $\mathbf{E}$. This is correct to first order in the potential difference between reservoirs and sufficient for analyzing the linear response regime. To determine potential we consider the deviation of particle density from its equlibrium value. Expanding the result in Eq.(2.6) in V and U, and neglecting second-order corrections, gives

$$\delta n(\mathbf{r}) = \nu \left(\frac{1}{2} - \frac{\theta_1(\mathbf{r}) - \theta_2(\mathbf{r})}{2\pi} \right) eV - \nu e U(\mathbf{r}), \tag{2.9}$$

where ν is the two-dimensional compressibility (which, for noninteracting fermions equals their density of states). The quasineutrality condition requires that the dependence $U(\mathbf{r})$ is such that $\delta n(\mathbf{r})$ vanishes, giving

$$U(\mathbf{r}) = \left(\frac{1}{2} - \frac{\theta_1(\mathbf{r}) - \theta_2(\mathbf{r})}{2\pi} \right) V. \tag{2.10}$$

The potential $U(\mathbf{r})$, shown in Fig.2-1 (b), rises gradually across the slit, forming a smooth step with the asymptotic values $\pm eV/2$ matching the values in reservoirs.

Under what conditions is the result in Eq.(2.10) valid? As the conventional wisdom has it, quasineutrality is obeyed at the lengthscales greater than the Thomas-Fermi (TF) screening radius. In our case this translates into the condition $w\kappa_{TF} \gg 1$ with $\kappa_{TF} = 2\pi e^2 \nu$ the two-dimensional TF screening parameter. The TF screening is enhanced in the presence of a proximal gate, in which case the distance to the gate acts as an effective TF radius. However, while this condition is necessary and sufficient in three dimensions, things may become more complicated in two dimensions. Indeed, imperfect screening of the long-range three-dimensional Coulomb potential by charges in a two-dimensional system generates power-law tails in the potential extending to the distances much greater than the TF radius. Poor screening may lead to deviation from charge neutrality. We will ignore these effects for the time being.

2.2 Viscous Electron Flow: Superballistic Transport

In this section we analyze hydrodynamic electron flow through the slit with the help of the Navier-Stokes equation. We will determine the flow and express the conductance through electron viscosity, deriving the result in Eq.(1.1). However, prior to diving into this analysis, it is useful to start with a general discussion of the conditions under which the hydrodynamic description of electron flows is valid.

The validity of hydrodynamics relies on the existence of locally conserved quantities. In our problem, particle number is conserved in all collisions. However, momentum conservation is approximate because translational symmetry is broken by lattice structure and by disorders and phonons. Momentum conservation is a good approximation so long as:

1. Disorder scattering and phonon scattering rates are much smaller than the ee scattering rate $\gamma_{ee} \gg \gamma_{ph}, \gamma_{disorder}$.

2. Umklapp scattering (that can change momentum by a reciprocal lattice vector) is weak.

3. In a realistic device there is momentum loss at the boundary, with a effective scattering rate $\gamma_{boundary} \approx v_F/w$, and hence we require $\gamma_{ee} \gg \gamma_{boundary}$.

The first condition can be fairly easily met in high-mobility electron systems such as graphene or two-dimensional electron gas in in GaAs. The second condition is fulfilled due to crystal lattice symmetry (in GaAs the carrier band is a small pocket positioned at the Γ point, in graphene it consists of two pockets at the points K and K' which are separated by a *third* of a reciprocal lattice vector). The validity of the third condition depends on temperature and it is that condition that determines the regime of the electron system. This condition can be rewritten as a competition between electron-electron mean free path l_{ee} and the slit width w, and hydrodynamic regime requires $l_{ee} \ll w$. Here we will not consider energy transport because in a degenerate Fermi system, $T \ll \epsilon_F$, it is a subleading effect to momentum and charge transport.

In this section, we will derive viscous conductance formula Eq.(1.1). In the hydrodynamic regime, the fluid should be described by the Navier-Stokes equation

$$\left(\partial_t + \mathbf{v}\cdot\nabla - \nu\nabla^2\right)\mathbf{v} = -\frac{1}{\rho}\nabla P. \tag{2.11}$$

Taken at face value this equation represents a formidable mathematical problem. Luckily, however, in our case there are some simplifications which make the problem tractable. Namely,

- We will only consider DC transport, so all time derivatives can be dropped.
- Due to the strong Coulomb repulsion, the electron fluid is effectively incompressible $\nabla\cdot\mathbf{v} = 0$.
- The electron fluid is highly viscous and thus the flow is laminar. Microscopic calculation of the kinematic viscosity yields $\nu = \frac{1}{4}v_F^2\gamma_{ee}^{-1} \sim 0.1\mathrm{m}^2/\mathrm{s}$, where $v_F \sim 10^6\mathrm{m/s}$ is the Fermi velocity and $\gamma_{ee} \sim 10^{13}\mathrm{s}^{-1}$ (at 100K) is the electron-electron scattering rate [19]. This value of viscosity is comparable to that of honey. The Reynolds number is defined as $\mathrm{Re} = v_F L/\nu$, where $L \sim 1\mu\mathrm{m}$ is the typical geometrical size of the device. For electron fluid Re values are at most $1-10$ or smaller, showing that the electron fluid moves as a laminar flow without generating turbulence. Intuitively, this is because electrons are light and hence inertia is not important. Therefore, nonlinear terms can be dropped.

Under these conditions the system can be described by the Stokes equation (a linearized Navier-Stokes equation) [32]

$$\eta\nabla^2\mathbf{v}(\mathbf{r}) = ne\nabla\phi(\mathbf{r}). \tag{2.12}$$

Here $\mathbf{v}(\mathbf{r})$ is the velocity field, which is related to current density by $\mathbf{j} = ne\mathbf{v}$, $\phi(\mathbf{r})$ is the electric potential, η is the viscosity and we have ignored ohmic resistivity due to impurity or phonon scattering.

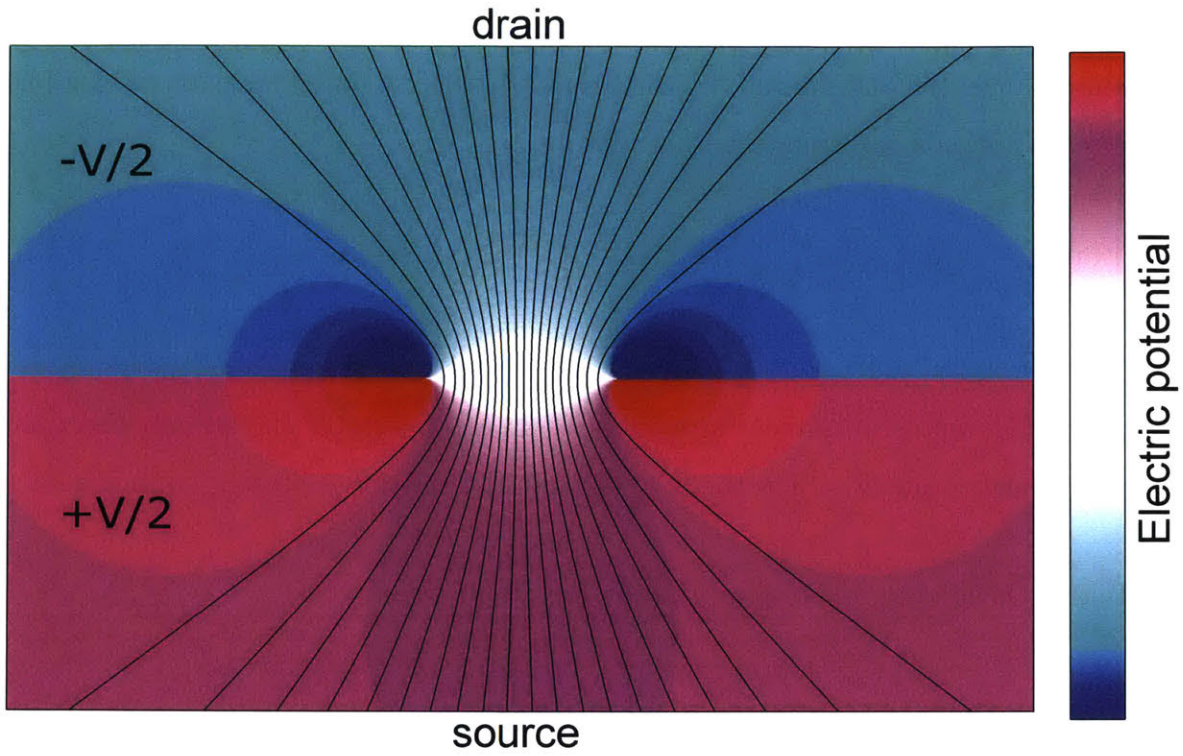

Figure 2-2: Current streamlines (black) and potential colormap for viscous flow through a slit. Velocity magnitude is proportional to the density of streamlines. Current forms a narrow stream, avoiding the boundaries where dissipation occurs and allowing the resistance, Eq.(1.1), to drop below the ballistic-limit value.

A general solution of the two-dimensional Stokes problem, Eq.(2.12), can be constructed by introducing the stream function through the relations $v_x = \partial_y \psi(\mathbf{r})$, $v_y = -\partial_x \psi(\mathbf{r})$ in order to resolve the incompressibility condition $\nabla \cdot \mathbf{v} = 0$. Plugging it in Eq.(2.12) and taking curl of both sides eliminates the pressure term and gives a biharmonic equation for the unknown function ψ:

$$(\partial_x^2 + \partial_y^2)^2 \psi(\mathbf{r}) = 0, \tag{2.13}$$

which must be solved with suitably chosen boundary conditions. A general complex-valued solution of this equation can be constructed as a sum $f_1(z) + \bar{z} f_2(z)$, where $f_{1,2}$ are analytic functions of a complex variable $z = x + iy$. The stream function is then obtained as $\psi = \mathrm{Re}\,(f_1(z) + \bar{z} f_2(z))$.

Applying this prescription to the slit geometry $-\frac{w}{2} < x < \frac{w}{2}$, $y = 0$, we seek a function that has an asymptotic behavior $\mathrm{Re}\,(i \log z)$ at large z (free flow at infinity)

and satisfies the no-slip conditions at the slit boundary $|x| > w/2$, $y = 0$, i.e. has vanishing tangential and normal derivatives for $y \to 0^{\pm}$. A closed-form expression for the stream function satisfying these conditions is

$$\psi(x,y) = A\,\mathrm{Re}\left[-i\log\left(z+\sqrt{z^2-\frac{w^2}{4}}\right)+i\bar{z}\left(\sqrt{z^2-\frac{w^2}{4}}-z\right)\frac{4}{w^2}\right]. \qquad (2.14)$$

The relation with the velocity field $v_x = \partial_y\psi(\mathbf{r})$, $v_y = -\partial_x\psi(\mathbf{r})$ means that the contours of ψ represent current streamlines. This property of the stream function helps to visualize the flow. For the flow through the slit this is illustrated in Fig.2-2.

Taking the stream function on the slit line $y = 0$ gives

$$\psi(-w/2 < x < w/2) = A\left(\arccos\left(\frac{2x}{w}\right) - x\sqrt{\frac{w^2}{4}-x^2}\right), \qquad (2.15)$$

and a constant at $|x| > w$. The relations $v_x = \partial_y\psi(\mathbf{r})$, $v_y = -\partial_x\psi(\mathbf{r})$ then give a semicircle distribution for current density inside the slit:

$$j_y(|x| < w/2) = neA\frac{16}{w^2}\sqrt{\frac{w^2}{4}-x^2}, \quad j_y(|x| > w/2) = 0. \qquad (2.16)$$

The flow is fast in the middle and slows down near the slit edges. This is distinct from current distribution for ballistic flow, which is flat inside the slit. Total current flowing through the slit, obtained by integrating the semicircle distribution for j_y or directly from the difference $\psi(x = w/2) - \psi(x = -w/2)$ is expressed as $I = \pi neA$.

Potential can now be found by plugging velocity $\mathbf{v}$, expressed through the stream function, into the Stokes equation. The first term in Eq.(2.14) is a harmonic function, and thus vanishes under Laplacian. We therefore obtain

$$A\eta\nabla\times\left((\partial_x^2+\partial_y^2)\mathrm{Re}\,i\bar{z}\sqrt{z^2-\frac{w^2}{4}}\frac{4}{w^2}\right) = ne\nabla\phi(\mathbf{r}). \qquad (2.17)$$

Expressing Laplacian through the ∂_z and $\partial_{\bar{z}}$ derivatives as $\partial_x^2+\partial_y^2 = (\partial_x+i\partial_y)(\partial_x -$

$i\partial_y) = 4\partial_z\partial_{\bar{z}}$, moving it under Re and evaluating the derivatives gives the relation

$$\frac{16A}{w^2}\eta\nabla\times\left(\mathrm{Re}\, i\frac{z}{\sqrt{z^2-\frac{w^2}{4}}}\right) = ne\nabla\phi(\mathbf{r}). \tag{2.18}$$

Finally, since derivatives of analytic functions obey $\partial_y f = i\partial_x f$, we can replace curl by a gradient and simultaneously drop an i. This gives the potential

$$\phi(\mathbf{r}) = -\frac{16I\eta}{\pi(ne)^2w^2}\,\mathrm{Re}\,\frac{z}{\sqrt{z^2-\frac{w^2}{4}}}, \tag{2.19}$$

where we plugged in the expression of A through the net current.

Now we can link the resistance of the slit with viscosity. Identifying the asymptotic values of potential $\phi(\mathbf{r})$ in the reservoirs above and below the slit with $\pm V/2$ gives a linear $I-V$ dependence

$$V = \frac{32\eta}{\pi(ne)^2w^2}\,I. \tag{2.20}$$

The I/V ratio then gives the conductance, Eq.(1.1). It is interesting to compare this result to the ballistic conductance $G_{\mathrm{ball}} = \frac{ge^2}{h}\frac{2w}{\lambda_F}$. Writing the dynamic viscosity as a product of kinematic viscosity and mass density, $\eta = \nu mn$, and using the relation $\nu = \frac{1}{4}v_F l_{\mathrm{ee}}$, derived below, we estimate

$$G_{\mathrm{vis}} \approx G_{\mathrm{ball}}\frac{\pi^2}{16}\frac{w}{l_{\mathrm{ee}}}. \tag{2.21}$$

Here l_{ee} is the mean free path for electron-electron collisions. In the hydrodynamic regime, $l_{\mathrm{ee}} \ll w$, this relation predicts conductance value above the ballistic value. The enhancement of conductance compared to the Landauer-Sharvin free-fermion conductance ("superballistic conduction") can be understood from the phase space argument discussed above. Alternatively it can be interpreted in terms of momentum relaxation slowing down in the hydrodynamic regime owning to a change in the typical particle trajectory length (namely, the zigzag paths terminating at the boundary being longer than the straight paths). The quadratic scaling $G_{\mathrm{vis}} \propto w^2$ is distinct from the

linear scaling $G_{\text{ball}} \propto w$ found in the ballistic regime. This scaling, as well as the higher-than-ballistic G values, can serve as a signature of a viscous flow.

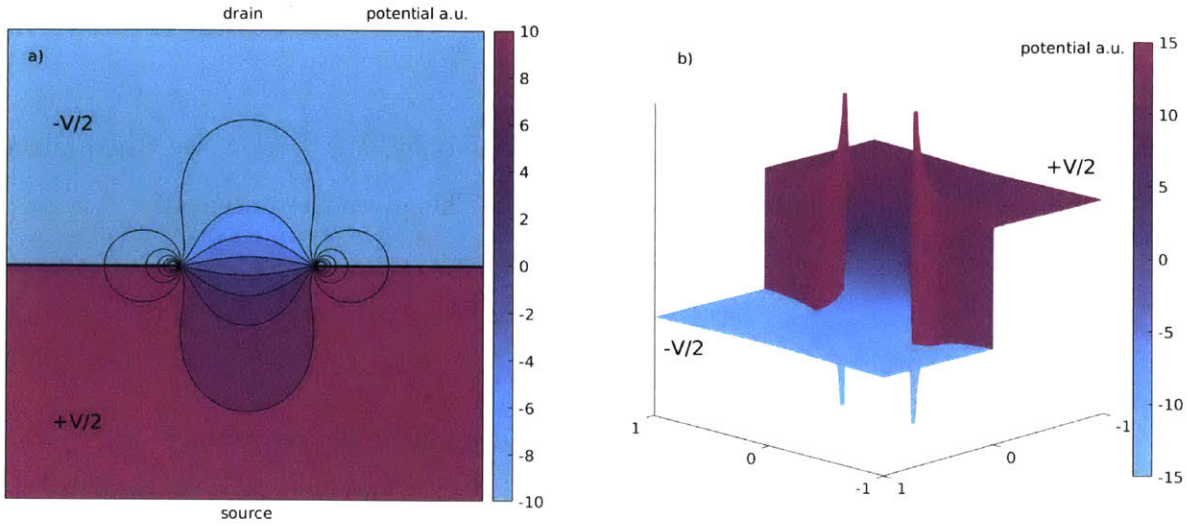

Figure 2-3: Potential for viscous flow through the slit. Potential spatial dependence is nonmonotonic, exhibiting peaks near the slit edges. Potential in the peaks is higher than potential of the source and lower than potential of the drain.

Another interesting aspect of viscous flow is the nonmonotonic character of the potential spatial dependence near the slit. Potential calculated from Eq.(2.19) is shown in Fig.2-3 as a contour plot (a) and a surface plot (b). This dependence is quite different from that predicted for ballistic flow, where potentoial drops monotonically along the current path. Here, in contrast, potential generates a field that, near the edge of the slit, is pointing opposite to current. The origin of this counterintuitive field direction can be understood in terms of a competition between drag due to flow in the bulk and the force due to momentum dissipation at the boundary which acts to stop the flow and thus generates an internal pressure gradient against the flow.

As illustrated in Fig.2-3, this leads to spikes near the slit edges, with the potential magnitude in the spikes exceeding that in the reservoirs. This interesting behavior, representing an up-converting DC-current transformer, arises due to the electric field pointing against the current near the viscous fluid edge [32]. A nonmonotonic potential inside the systems with values that exceed the source and the drain potential is another signature of hydrodynamic flows.

There are several validity conditions for these results. One is that the system

is in the hydrodynamic regime i.e. the ee collisions dominate over other scattering processes. Furthermore, we assume that the constriction width w is much greater than the ee scattering mean free path l_{ee} and smaller than the mean free path for momentum-nonconserving scattering by disorder, phonons, etc. Another requirement is quasineutrality, incorporated in our solution of Stokes equation through the incompressibility condition $\nabla \cdot \mathbf{v} = 0$. As discussed at the end of Sec.2.1, quasineutrality holds, in general, at the lengthscales greater than the Thomas-Fermi screening length (with additional caveats arising in two-dimensional systems due to the poor screening of $1/r$ interactions). In practical terms, this means that the spikes in the potential in Fig.2-3, rather than being perfectly sharp, will be smeared out. The spike width will be set by the screening length or the mean free path l_{ee}, whichever is greater.

Chapter 3

Theory of Electron Flow at the Ballistic-to-Hydrodynamic Crossover

3.1 The Boltzmann Equation Model

Here we present a theory of the ballistic-to-viscous crossover for a flow through the slit geometry. Since we are interested in the linear response, we use the kinetic equation linearized in deviations of particle distribution from the equilibrium Fermi step (assuming $k_{\mathrm{B}}T \ll E_F$),

$$(\partial_t + \mathbf{v}\nabla_{\mathbf{x}})\, f(\theta, \mathbf{x}, t) = I_{\mathrm{ee}}(f) + I_{\mathrm{bd}}(f), \tag{3.1}$$

where θ is the angle parameterizing particle momentum at the 2D Fermi surface. By assuming that Fermi-liquid theory applies, all relevant momenta are on the fermi-level and we can neglect energy dependence of f. Here I_{ee} and I_{bd} describe momentum-conserving carrier collisions and momentum-nonconserving scattering at the boundary, respectively.

In the presence of momentum-conserving collisions transport is succinctly described by *quasi-hydrodynamic variables* defined as deviations in the average particle density and momentum from local equilibrium [30]. These quantities can be expressed

as angular harmonics of the distribution $f(\theta, \mathbf{x}, t)$:

$$f_0 = \langle f(\theta) \rangle_\theta , \quad f_{\pm 1} = \left\langle e^{\mp i\theta} f(\theta) \right\rangle_\theta , \tag{3.2}$$

where we introduced notation $\langle ... \rangle_\theta = \oint ... \frac{d\theta}{2\pi}$. The quantities f_0, $f_{\pm 1}$, conserved in the ee collisions, represent the zero modes of $I_{\rm ee}$. For suitably chosen $I_{\rm ee}$ the task of solving the kinetic equation in a relatively complicated slit geometry is reduced to analyzing a selfconsistency equation for the variables f_0, $f_{\pm 1}$. We will derive a linear integral equation for these quantities, and solve it to obtain the current density, the potential and the conductance.

To facilitate the analysis, we model $I_{\rm ee}$ by choosing a single relaxation rate for all non-conserved harmonics:

$$I_{\rm ee}(f) = -\gamma(f - Pf), \quad P = \sum_{m=0,\pm 1} |m\rangle \langle m| , \tag{3.3}$$

where γ represents the ee collision rate, with $l_{\rm ee} = v/\gamma$, and P is a projector in the space of angular harmonics of $f(\theta)$ that selects the harmonics conserved in ee collisions. Here we introduced Dirac notation for $f(\theta)$ with the inner product $\langle f_1 | f_2 \rangle = \oint \frac{d\theta}{2\pi} \bar{f}_1(\theta) f_2(\theta)$. Namely,

$$\langle \theta | m \rangle = e^{im\theta}, \quad Pf(\theta) = \sum_{m=0,\pm 1} \oint \frac{d\theta'}{2\pi} e^{im(\theta-\theta')} f(\theta').$$

As in quantum theory, the Dirac notation proves to be a useful bookkeeping tool to account on equal footing for the distribution function position and wavenumber dependence, as well as the angle dependence.

To simplify our analysis we replace the slit geometry by that of a full plane, with a part of the line $y = 0$ made impenetrable through a suitable choice of $I_{\rm bd}(f)$. Scattering by disorder at the actual boundary conserves f_0 but not $f_{\pm 1}$. We can

therefore model momentum loss due to collisions at the boundary using

$$I_{\mathrm{bd}}(f) = -\alpha(\mathbf{x})P'f, \quad \alpha(\mathbf{x}) = \begin{cases} 0, & |x| < \frac{w}{2} \\ b\delta(y), & |x| \geq \frac{w}{2} \end{cases}, \tag{3.4}$$

where P' is a projector defined in a manner similar to P, projecting f on the harmonics $m = \pm 1$. The term $\alpha(x)$ describes momentum relaxation on the line $y = 0$, equal zero within the slit and b outside. The parameter $b > 0$ with the dimension of velocity, introduced for mathematical convenience, describes partially transparent boundary. An impenetrable no-slip boundary, which corresponds to the situation of interest, can be modeled by taking the limit $b \to \infty$.

We will analyze the flow induced by a current applied along the y direction, described by a distribution

$$f(\theta, \mathbf{x}) = f^{(0)}(\theta) + \delta f(\theta, \mathbf{x}), \quad f^{(0)}(\theta) \sim \sin\theta. \tag{3.5}$$

Here $f^{(0)}$ and δf, which we will also write as $\left|f^{(0)}\right\rangle$ and $|\delta f\rangle$, represent a uniform current-carrying state and its distortion due to scattering at the $y = 0$ boundary. Once found, the spatial distribution $f(\theta, \mathbf{x})$ will allow us to determine the resulting potential and resistance. The kinetic equation, Eq.(3.1), reads

$$\left(\partial_t + K + \alpha(\mathbf{x})P'\right)|f\rangle = 0, \quad K = \mathbf{v}\nabla + \gamma\hat{1} - \gamma P, \tag{3.6}$$

From now on we suppress the coordinate and angle dependence of f and use the Dirac notation. Plugging $f = f^{(0)} + \delta f$, we rewrite Eq.(3.6) as $(K + \hat{\alpha})\,|\delta f\rangle = -\hat{\alpha}\left|f^{(0)}\right\rangle$, where, for conciseness, we absorbed the projector P' into $\hat{\alpha}$ and set $\partial_t f = 0$ for a steady state. We write a formal operator solution as

$$|\delta f\rangle = -(1 + G\hat{\alpha})^{-1} G\hat{\alpha}\left|f^{(0)}\right\rangle, \tag{3.7}$$

where $G = K^{-1}$ is the Green's function. Performing analysis in momentum represen-

tation, we treat the scattering term in Eq.(3.4) as an operator

$$\langle \mathbf{k}|\hat{\alpha}|\mathbf{k}'\rangle = P'\alpha_{k_1-k_1'}, \quad \alpha_k = 2\pi b\delta(k) - bw\,\mathrm{sinc}\,\frac{kw}{2}, \tag{3.8}$$

where $\mathrm{sinc}\,x = \frac{\sin x}{x}$. The two terms in α_k describe scattering at the $y = 0$ line less the slit contribution.

Next we derive a closed-form integral equation for quasi-hydrodynamic variables. This is done by projecting the quantities in Eq.(3.7) on the $m = 0, \pm 1$ harmonics, Eq.(3.2). Acting on Eq.(3.7) with P gives $|P\delta f\rangle = -(1 + \tilde{G}\hat{\alpha})^{-1}\tilde{G}\hat{\alpha}\left|f^{(0)}\right\rangle$ where $\tilde{G} = PGP$ is a 3×3 matrix in the $m = 0, \pm 1$ space (here we used the identity $\hat{\alpha} = P\hat{\alpha}P$ which follows from $PP' = P'P = P'$). The integral equation is obtained by acting on both sides with the operator $1 + \tilde{G}\hat{\alpha}$, giving

$$(1 + \tilde{G}\hat{\alpha})\left|\tilde{f}\right\rangle = \left|f^{(0)}\right\rangle. \tag{3.9}$$

Here we defined $\tilde{f} = f^{(0)} + P\delta f$, the full distribution function projected on the $m = 0, \pm 1$ harmonics.

The quantity $\tilde{f}$ represents an unknown function which can be found, in principle, by inverting the integral operator $1+\tilde{G}\alpha$ in Eq.(3.9). However, rather than attempting to invert $1 + \tilde{G}\alpha$ directly in 2D, it is more convenient to proceed in two steps: first analyze Eq.(3.9) in 1D, on the line $y = 0$, and then extend the solution into 2D.

3.2 Green's Function

We start with finding $\tilde{G}$, the Green's function of the system. As a first step, we evaluate the 3×3 matrix $S = \gamma P G_0 P$ where $G_0 = 1/(i\mathbf{kv} + \gamma)$. The quantity G_0 is an auxiliary Green's function describing transport in which all harmonics, including $m = 0, \pm 1$, relax at a rate γ. Direct calculation gives matrix elements (here $m, m' = 0, \pm 1$, $\Delta m = m' - m$):

$$S_{mm'} = \left\langle \frac{\gamma e^{i(m'-m)\theta}}{\gamma + i\mathbf{kv}} \right\rangle_\theta = \tanh\beta \frac{e^{i\theta_k \Delta m}}{(ie^{\beta})^{|\Delta m|}}, \tag{3.10}$$

where we denote $\sinh\beta = \frac{\gamma}{kv}$ and $\theta_k = \arg(k_1 + ik_2)$.

The matrix $\tilde{G}$ can now be expressed through the matrix S by expanding the actual Green's function as $G = 1/(G_0^{-1} - \gamma P) = G_0 + G_0\gamma P G_0 + ...$, which gives

$$G = G_0 + G_0 T G_0, \quad T = \frac{\gamma P}{1 - \gamma P G_0 P}. \tag{3.11}$$

Here we re-summed the series, expressing the result in terms of a 3×3 matrix T in a manner analogous to the derivation of the Lippmann-Schwinger T-matrix for quantum scattering with a finite number of 'active' channels. We note that $\gamma P G_0 P$ is nothing but the matrix S in Eq.(3.10). Plugging Eq.(3.11) into $\tilde{G} = PGP$ and performing a tedious but straightforward matrix inversion we obtain

$$\tilde{G} = \frac{\gamma^{-1}S}{1-S} = \frac{\sinh\beta}{\gamma}\begin{pmatrix} e^{\beta} & -i\bar{z}_k & -e^{\beta}\bar{z}_k^2 \\ -iz_k & e^{-\beta} & -i\bar{z}_k \\ -e^{\beta}z_k^2 & -iz_k & e^{\beta} \end{pmatrix}, \tag{3.12}$$

where $z_k = e^{i\theta_k}$ and the basis vectors are ordered as $|+1\rangle$, $|0\rangle$, $|-1\rangle$.

In what follows it will be convenient to transform $|\pm 1\rangle$ to the even/odd basis $|c\rangle = \frac{|+1\rangle+|-1\rangle}{\sqrt{2}}$, $|s\rangle = \frac{|+1\rangle-|-1\rangle}{\sqrt{2}i}$. In this basis $\tilde{G}$ reads

$$\begin{pmatrix} \tilde{G}_{00} & \tilde{G}_{0c} & \tilde{G}_{0s} \\ \tilde{G}_{c0} & \tilde{G}_{cc} & \tilde{G}_{cs} \\ \tilde{G}_{s0} & \tilde{G}_{sc} & \tilde{G}_{ss} \end{pmatrix} = \begin{pmatrix} \frac{R_-}{\gamma\kappa^2} & \frac{-i\sqrt{2}\kappa_1}{\gamma\kappa^2} & \frac{-i\sqrt{2}\kappa_2}{\gamma\kappa^2} \\ \frac{-i\sqrt{2}\kappa_1}{\gamma\kappa^2} & \frac{2\kappa_2^2 R_+}{\gamma\kappa^4} & \frac{-2\kappa_1\kappa_2 R_+}{\gamma\kappa^4} \\ \frac{-i\sqrt{2}\kappa_2}{\gamma\kappa^2} & \frac{-2\kappa_1\kappa_2 R_+}{\gamma\kappa^4} & \frac{2\kappa_1^2 R_+}{\gamma\kappa^4} \end{pmatrix}, \tag{3.13}$$

where the basis vectors are ordered as $|0\rangle$, $|c\rangle$, $|s\rangle$ and we defined $R_\pm(\kappa) = \sqrt{\kappa^2+1}\pm 1$ and $\kappa_{1,2} = \frac{v}{\gamma}k_{1,2}$, $\kappa = \sqrt{\kappa_1^2 + \kappa_2^2}$. The quantities G and $\tilde{G}$ represent, through their dependence on $\mathbf{k}$, translationally invariant integral operators in position representation and diagonal operators in momentum representation.

3.3 Hydrodynamic Modes, Calculation of Viscosity

As a sanity check of the above formalism, we demonstrate the hydrodynamic modes, and relate the collision rate γ to the kinematic viscosity ν.

We reinstall the time dependence into the free space Boltzmann equation as the following:

$$(\hat{K} - \gamma P)f = 0, \quad \hat{K} = \partial_t + \mathbf{v}\nabla_{\mathbf{x}} + \gamma\hat{1}. \tag{3.14}$$

Since f_0 and $f_{\pm 1}$ are zero modes of the collision operator I_{ee}, they dominate at low frequencies and long wavelengths. Accordingly, we can obtain hydrodynamic modes from plane-wave solutions, $f(\theta, \mathbf{x}, t) \sim f(\theta)e^{-i\omega t + i\mathbf{kx}}$.

Using the same techniques as the previous section, we can calculate the Green's function of Eq.(3.14) to be

$$\tilde{G} = \frac{\gamma^{-1}g}{1-g}. \tag{3.15}$$

Here the 3 by 3 matrix $g = \gamma P\hat{K}^{-1}P$ has matrix elements

$$g_{mm'} = \langle m|\, \gamma P\hat{K}^{-1}P\, |m'\rangle = \left\langle \frac{\gamma e^{i(m'-m)\theta}}{\gamma_\omega + i\mathbf{kv}} \right\rangle_\theta = \tanh\beta \frac{\gamma e^{i\theta_k \Delta m}}{\gamma_\omega \left(ie^{\beta}\right)^{|\Delta m|}}, \tag{3.16}$$

which differs from Eq.(3.10) in that γ in the denominator is replaced by $\gamma_\omega = \gamma - i\omega$.

Low energy excitations of the system are given by poles of the Green's function $\tilde{G}$, which only occurs if the denominator $1 - g$ vanishes. In other words, the matrix g must have eigenvalue 1:

$$f_m = \sum_{m'=-1}^{1} g_{mm'} f_{m'}. \tag{3.17}$$

As we now show, Eq.(3.17) generates an acoustic and a viscous mode. Since the acoustic and the viscous modes are longitudinal and transverse, respectively, it is convenient to do the analysis by performing an orthogonal transformation to the even/odd basis

$$|0\rangle, \quad |c\rangle = \frac{|1_k\rangle + |-1_k\rangle}{\sqrt{2}}, \quad |s\rangle = \frac{|1_k\rangle - |-1_k\rangle}{\sqrt{2}i}, \tag{3.18}$$

where we use notation $|m_k\rangle = e^{-im\theta_k}|m\rangle$. The modes $|c\rangle$ and $|s\rangle$ correspond to normalized angular harmonics $f_c(\theta) = \sqrt{2}\cos\tilde{\theta}$ and $f_s(\theta) = \sqrt{2}\sin\tilde{\theta}$, where $\tilde{\theta} = \theta - \theta_k$.

This transformation brings the 3×3 matrix $g_{mm'}$ to a block-diagonal form

$$\begin{pmatrix} g_{00} & g_{0c} & 0 \\ g_{c0} & g_{cc} & 0 \\ 0 & 0 & g_{ss} \end{pmatrix}. \tag{3.19}$$

For the odd-mode 1×1 block we find $g_{ss} = \frac{\gamma}{\gamma_\omega}\tanh\beta(1 + e^{-2\beta})$. Writing the dispersion relation $1 = g_{ss}$ and Taylor-expanding in small ω and k yields a viscous mode dispersing as

$$\omega = -i\nu k^2, \quad \nu = v^2/4\gamma. \tag{3.20}$$

Here ν is the viscosity defined so that the dispersion in Eq.(3.20) agrees with that obtained from the linearized Navier-Stokes equation $(\partial_t - \nu\nabla^2)\mathbf{v} = -\nabla P$.

The acoustic mode can be obtained from the even-mode 2×2 block

$$\begin{pmatrix} g_{00} & g_{0c} \\ g_{c0} & g_{cc} \end{pmatrix} = \frac{\gamma\tanh\beta}{\gamma_\omega}\begin{pmatrix} 1 & -i\sqrt{2}e^{-\beta} \\ -i\sqrt{2}e^{-\beta} & 1 - e^{-2\beta} \end{pmatrix}. \tag{3.21}$$

The dispersion relation $\det(1 - g) = 0$ gives

$$\left(\frac{\gamma_\omega}{\gamma\tanh\beta} - 1\right)\left(\frac{\gamma_\omega}{\gamma\tanh\beta} - 1 + e^{-2\beta}\right) + 2e^{-2\beta} = 0. \tag{3.22}$$

Plugging $\sinh\beta = \frac{\gamma}{kv}$, simplifying and Taylor-expanding in ω and k, yields a damped acoustic mode

$$\omega = \frac{1}{\sqrt{2}}kv - \frac{i}{2}\nu k^2, \tag{3.23}$$

where we expressed damping through viscosity ν, evaluated in Eq.(3.20).

3.4 Projecting to a 1D Problem

We now continue the analysis of Eq.(3.9), by projecting it down to the line $y = 0$.

First, we evaluate the matrix that represents the operator $\tilde{G}$ restricted to the line $y = 0$,

$$D(k_1) = \int_{-\infty}^{\infty} \frac{dk_2}{2\pi} \tilde{G}(k_1, k_2). \tag{3.24}$$

The matrix elements $\tilde{G}_{0c}$ and $\tilde{G}_{0s}$ are odd in k_2 and therefore give zero upon integration in Eq.(3.24). This gives a block-diagonal matrix

$$D(k_1) = \begin{pmatrix} D_{00}(k_1) & D_{0c}(k_1) & 0 \\ D_{c0}(k_1) & D_{cc}(k_1) & 0 \\ 0 & 0 & D_{ss}(k_1) \end{pmatrix}. \tag{3.25}$$

The quantity $D_{ss}(k_1)$ will play a central role in our analysis. Indeed, since the flow of interest is symmetric under $y \to -y$ and $x \to -x$, the $\tilde{f}_0$ and $\tilde{f}_c$ components vanish on the $y = 0$ line. As a result, the distribution function at $y = 0$ is of a pure $|s\rangle$ form i.e. $\tilde{f}(\theta, x) = g(x)\sqrt{2}\sin\theta$.

Evaluating the integral over k_2 in Eq.(3.24) we obtain

$$D_{ss}(k) = \frac{\frac{\pi}{2}\operatorname{sgn}\kappa + \kappa + (\kappa^2 + 1)\cot^{-1}\kappa}{\pi\kappa v}, \tag{3.26}$$

where $\kappa = kv/\gamma$. This expression defines an even function of k with the asymptotics

$$D_{ss}(|k|v \ll \gamma) = \frac{\gamma}{|k|v^2}, \quad D_{ss}(|k|v \gg \gamma) = \frac{2}{\pi v}. \tag{3.27}$$

Since the matrix element D_{ss} is an eigenvalue of D for the eigenvector $|s\rangle$, the θ dependence can be factored out of Eq.(3.9), giving $(1 + D\alpha)\,|g\rangle = |g^{(0)}\rangle$. Finally, multiplying by D^{-1}, we obtain the "central equation"

$$D_{ss}^{-1}(k) g_k + \int \frac{dk'}{2\pi} \alpha_{k-k'} g_{k'} = 2\pi\mu\delta(k), \tag{3.28}$$

where μ is an unspecified number, akin to a Lagrange multiplier, which fixes the total current value. Here, we wrote the relation $(D^{-1} + \alpha)\,|g\rangle = \mu\,|k = 0\rangle$ as an integral equation, replacing k_1 with k for clarity.

The origin of the μ-term in (3.28), and its relation with the properties of the operator D, is simplest to understand using a discretized momentum representation. Letting $k_1 = \frac{2\pi}{L}n$ and replacing

$$\int dk_1 ... \to \frac{2\pi}{L}\sum_n ..., \quad 2\pi\delta(k) \to L\delta_{k,0}, \tag{3.29}$$

i.e. putting the problem on a cylinder of circumference L, we see that the values $\tilde{G}_{ss}(k_1, k_2)$ vanish for $k_1 = 0$ and any k_2. This means that $D_{ss}(k_1)$ also vanishes for $k_1 = 0$ and thus the operator D does not have an inverse [1]. In this case caution must be exercised when multiplying by D^{-1}. Namely, the quantities $D^{-1}|f\rangle$ are defined modulo a null vector of D, which is the $k_1 = 0$ mode with an unspecified coefficient, represented by the μ-term. We note parenthetically that discretization has no impact on the values $D_{ss}(k_1 \neq 0)$ given in Eqs.(3.26),(3.27).

We obtain current distribution by solving numerically Eq.(3.28), discretized as in Eq.(3.29), and subsequently Fourier-transforming g_k to position space. The details of the numerical analysis will be discussed later. The resulting distribution, shown in Fig.3-1, features interesting evolution under varying γ: flat at small γ, the distribution gradually bulges out as γ increases, peaking at $x = 0$ and dropping to zero near $x = \pm\frac{w}{2}$. In the limit $\gamma \gg v/w$ it evolves into a semicircle coinciding with the hydrodynamic result, Eq.(2.16). Current suppression near the slit edges is in agreement with the streaming picture discussed above.

The solution on the line $y = 0$ can now be used to determine the solution in the bulk. E.g. to obtain the density $f_0(\mathbf{x})$ we project the relation (3.9) on $m = 0$ harmonic, taking into account that both $f^{(0)}$ and $\alpha\tilde{f}$ are of an $|s\rangle$ form. This allows to express the 2D density as $f_0(\mathbf{x}) = -\int dx'\tilde{G}_{0s}(\mathbf{x}, x')\alpha(x')g(x')$, with $\mathbf{x}$ a 2D coordinate and $-\infty < x' < \infty$. To avoid handling the $b \to \infty$ limit in α, we write this relation using Eq.(3.28) as

$$f_0(\mathbf{x}) = -\int dx'\tilde{G}_{0s}(\mathbf{x}, x')\left(\mu - \left(D_{ss}^{-1}g\right)(x')\right). \tag{3.30}$$

[1] However, according to Eq.(3.26), $D_{ss}(0)$ seems to be infinity. This puzzle can be solved by adding an infinitesimal momentum relaxation rate to the system, see Section 3.7.

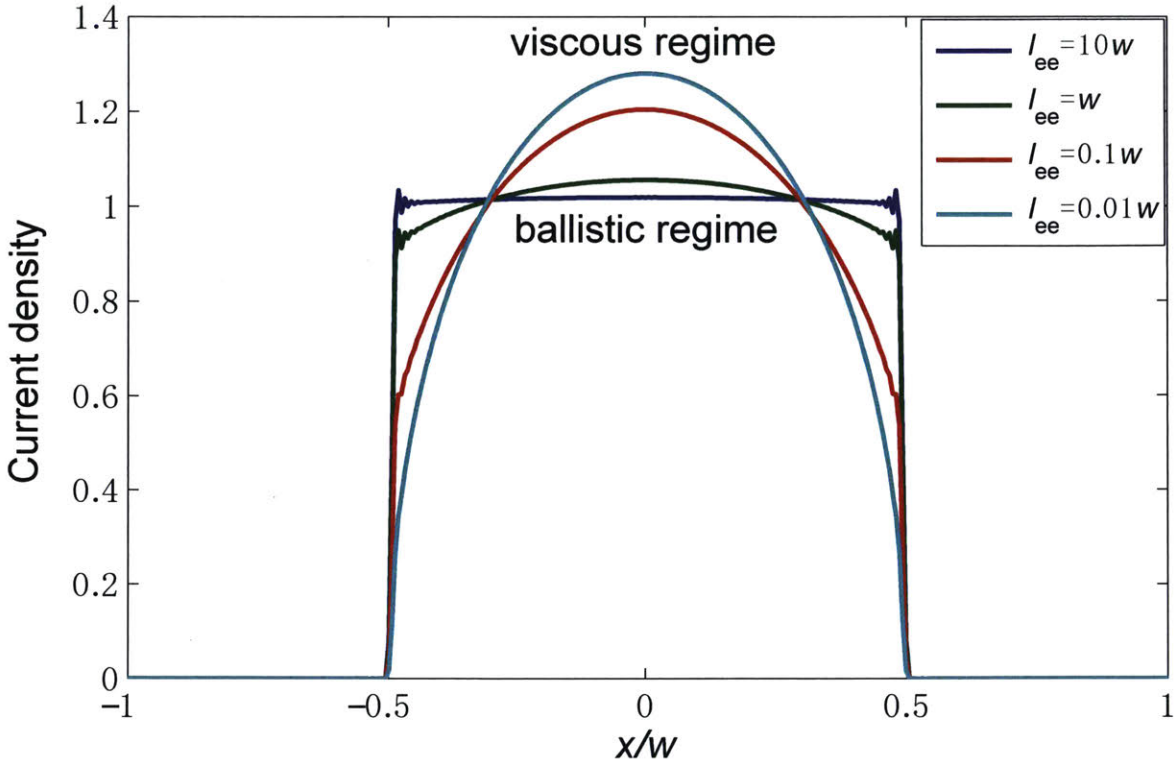

Figure 3-1: Current distribution in the slit for different carrier collision mean-free-path values. The total current is normalized to 1. The distribution evolves from a constant in the ballistic regime to a semicircle in the viscous regime, Eq.(2.16), illustrating the interaction-induced streaming effect. Parameters used: $L = 3w$, $b = 10^5 v$. A Fourier-space filter was used to smooth out the Gibbs phenomenon.

Plugging $\tilde{G}_{0s}(\mathbf{k}) = \frac{-i\sqrt{2}k_2}{v(k_1^2+k_2^2)}$, Fourier-transforming, and carrying out the k_2 integral by the residue method, $\int dk_2 e^{ik_2 y} \frac{ik_2}{k_1^2+k_2^2} = -\pi e^{-|yk_2|}\operatorname{sgn} y$, we obtain

$$f_0(\mathbf{x}) = \frac{\operatorname{sgn} y}{\sqrt{2}v} \int \frac{dk_1}{2\pi} e^{ik_1 x - |k_1 y|} \left(D_{ss}^{-1}(k_1) g_{k_1} - 2\pi\mu\delta(k_1) \right). \tag{3.31}$$

The resulting distributions, shown in Fig.3-2, are step-like. At large y the μ-term dominates, giving $f_0(|\mathbf{x}| \gg w) \approx -\frac{\mu}{\sqrt{2}v} \operatorname{sgn} y$. Therefore, the step height equals $\frac{\sqrt{2}}{v}\mu$ regardless of the parameter values used.

This relation provides a route to evaluate resistance. Namely, because of charge neutrality, the density f_0 obtained from a noninteracting model translates directly into potential distribution $\phi(\mathbf{x}) = \frac{1}{e\nu_0} f_0(\mathbf{x})$, where ν_0 is the density of states. Dividing the potential difference $V = \frac{\sqrt{2}\mu}{e\nu_0 v}$ by the total current $I = \int dx g(x) \langle ev \sin\theta | s \rangle = \frac{ev}{\sqrt{2}} g_{k_1=0}$,

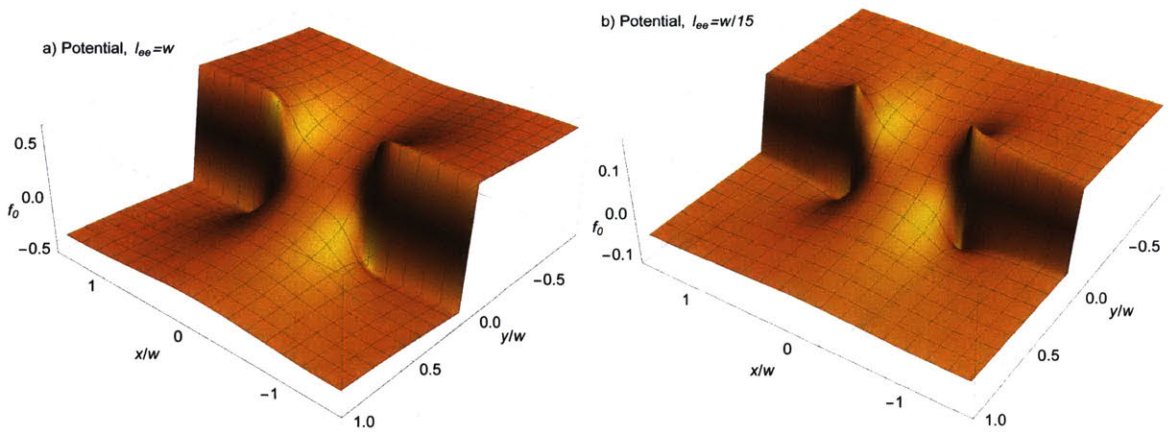

Figure 3-2: Potential distribution induced by current through a slit (a) at the crossover, $l_{ee} \sim w$, and (b) in the viscous regime, $l_{ee} \gg w$. The spikes at the slit edges in b) is a signature of a hydrodynamic behavior, see Eq.(2.19) and accompanying text. Plotted is particle density deviation from equilibrium, $f_0(\mathbf{x})$, which is proportional to potential (see text). Parameters used: (a) $\gamma = v/w$, (b) $\gamma = 15v/w$; other parameter values are the same as in Fig.3-1.

yields a simple expression for resistance

$$R = \frac{\mu\rho_*}{v g_{k=0}}, \quad \rho_* = \frac{2}{e^2 v \nu_0}, \tag{3.32}$$

where $g_{k=0} = \int g(x)dx$ and ρ_* is a constant of dimension Ohm $\cdot$ cm. Since $g \propto \mu$, the resulting R values are μ-independent. Fig.3-3a shows R plotted vs. γ. As expected, R decreases as γ increases, i.e. carrier collisions enhance conduction.

3.5 Analytic Solution of the Central Equation

In this section, we discuss the ballistic and the hydrodynamic limits of the central equation Eq.(3.28), which turn out to be analytically solvable.

The integral equation (3.28), which describes the current distribution in the slit, is defined on a line $-\infty < x < \infty$ in position representation. It reads

$$\alpha(x)g(x) + \int_{-\infty}^{\infty} dx' D_{ss}^{-1}(x-x')g(x')dx' = \mu, \tag{3.33}$$

$$D_{ss}^{-1}(x-x') = \int \frac{dk}{2\pi} \frac{e^{ik(x-x')}}{D_{ss}(k)}, \quad \alpha(x) = \begin{cases} b, & |x| > \frac{w}{2} \\ 0, & |x| < \frac{w}{2} \end{cases}$$

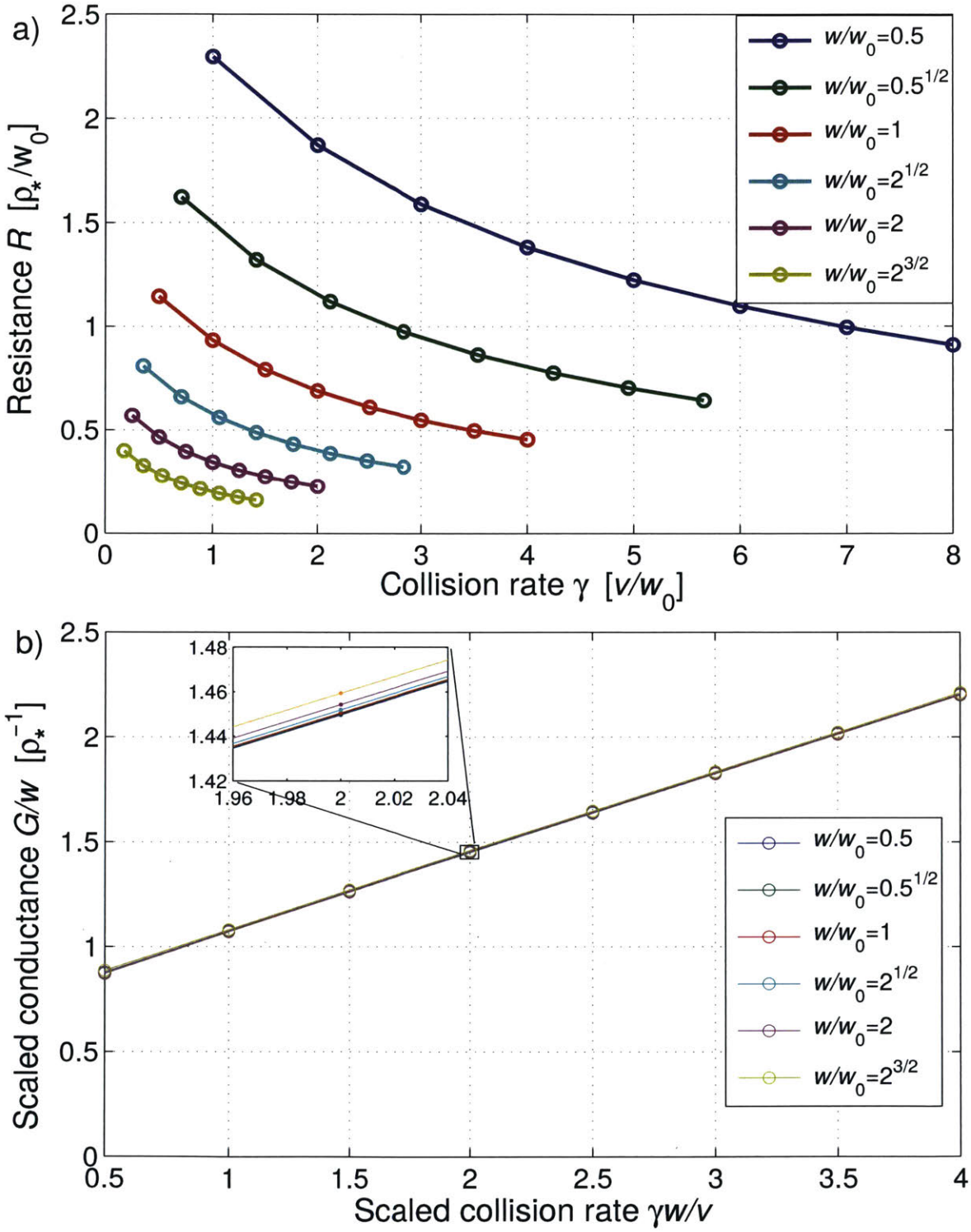

Figure 3-3: a) The resistance R, Eq.(3.32), plotted vs. γ. Upon rescaling $R \to Rw$, $\gamma \to \gamma w$ all the curves collapse on one curve, confirming that the only relevant parameter is the ratio $w/l_{\rm ee} = w\gamma/v$. b) Scaled conductance $G = 1/(Rw)$ vs. γw. All curves collapse onto a single straight line, which can be fitted with $(0.694 + 0.378\gamma w)\rho_*^{-1}$. Parameters used: $b = 10^6 v$, the number of sampling points within the slit ~ 160, the length unit $w_0 = \frac{1}{30}L$.

The ballistic and the hydrodynamic regimes are described by the large-k and small-k limits of $D_{ss}(k)$ respectively, given in Eq.(3.27).

3.5.1 Ballistic Limit

We consider the near-collisionless limit $\gamma \ll v/w$. In this case $D_{ss}(k) \approx 2/\pi v$ and the integral equation (3.28) turns into an algebraic equation which is solved by a step-like distribution

$$g(|x| > w/2) = \frac{2\mu}{\pi v + 2b}, \quad g(|x| < w/2) = \frac{2\mu}{\pi v}. \tag{3.34}$$

In the limit $b \to \infty$ the total current is $I = \frac{ev}{\sqrt{2}} \frac{2w\mu}{\pi v}$. Taking the 2D density of states $\nu_0 = \frac{Nm}{2\pi\hbar^2}$ (here N is spin-valley degeneracy, e.g. $N = 4$ for graphene), we find

$$R = \frac{V}{I} = \frac{1}{N} \frac{h}{e^2} \frac{\lambda_F}{2w}, \quad \lambda_F = \frac{2\pi}{k_F}. \tag{3.35}$$

This is precisely the collisionless Landauer value. Spatial dependence can be obtained by plugging $g(x)$ in Eq.(3.31). Integrating and taking the limit $b \to \infty$ gives

$$f_0(\mathbf{x}) = -\frac{\operatorname{sgn} y}{\sqrt{2}v} \mu \left(1 - \frac{1}{\pi}\theta(\mathbf{x})\right), \tag{3.36}$$

where $\theta(\mathbf{x}) = \tan^{-1} \frac{|y|w}{x^2+y^2-\frac{1}{4}w^2}$ is the angle at which the interval $[-\frac{w}{2}, \frac{w}{2}]$ is seen from the point $\mathbf{x} = (x, y)$. This agrees with Fig.2-1 and confirms the result $\frac{\mu}{\sqrt{2}v}$ for the step height.

3.5.2 Hydrodynamic Limit

In the hydrodynamic limit, $\gamma \gg v/w$ and $D_{ss}(k) = \frac{\gamma}{|k|v^2}$, we fourier transform D_{ss} back to position representation:

$$\begin{aligned} D_{ss}^{-1}(x - x') &= \int_{-\infty}^{\infty} \frac{dk}{2\pi} \frac{|k|v^2}{\gamma} e^{ik(x-x')} \\ &= -\frac{v^2}{2\pi\gamma} \left(\frac{1}{(x - x' + i0)^2} + \frac{1}{(x - x' - i0)^2} \right). \end{aligned} \tag{3.37}$$

This coincides with the kernel that relates potential in the plane and current on the slit line, derived in Ref.[34] from a hydrodynamic approach (Stokes equation combined with the incompressibility condition). We will now show that the integral equation (3.33), in the limit $b \to \infty$, is satisfied by a semicircle solution identical to that found by an electrostatic method. The analysis is facilitated by representing the semicircle solution, with a yet-undetermined normalization factor, as

$$g(x) = a\sqrt{1 - \frac{4x^2}{w^2}} = \text{Im}\, f_+(z) - \text{Im}\, f_-(z), \quad z = \frac{2x}{w}, \tag{3.38}$$

where $f_\pm(z)$ are given by $\frac{a}{2}(\sqrt{z^2-1} - z)$ continued from large z to $-1 < z < 1$ through the upper or lower complex z halfplane, respectively. Using this representation and the expression in Eq.(3.37), we can carry out the integral in Eq.(3.33) by the method of residues, closing the integration path through the upper halfplane for $f_+(z)$ and the lower halfplane for $f_-(z)$. The contributions of large z drop out since the functions $f_\pm(z)$ vanish at infinity, giving

$$\begin{aligned} &\int_{-\infty}^{\infty} dx' D_{ss}^{-1}(x - x') g(x') dx' \\ &= \text{Im}\left[\frac{2iv^2}{\gamma w}(f'_+(z) - f'_-(z))\right]\Bigg|_{-\infty}^{\infty} = \frac{2v^2 a}{\gamma w}. \end{aligned} \tag{3.39}$$

Here we have taken x to be in the interval $[-\frac{w}{2}, \frac{w}{2}]$. Inserting this result in Eq.(3.33) we determine the normalization factor $a = \frac{\gamma w}{2v^2}\mu$. The resistance is obtained by evaluating

$$g_{k=0} = \int_{-\frac{w}{2}}^{\frac{w}{2}} g(x) dx = \frac{\pi}{4} w a,$$

and plugging it in Eq.(3.32). This gives

$$R = \frac{8v\rho_*}{\pi\gamma w^2} = \frac{16}{\pi e^2 \gamma w^2 \nu_0}.$$

Writing the 2D density of states as $\nu_0 = \frac{Nm}{2\pi\hbar^2} = \frac{2n}{mv^2}$ and expressing γ through viscosity $\eta = nmv^2/4\gamma$ [see Eq.(3.20)] we find

$$R = \frac{8mv^2}{\pi e^2 \gamma w^2 n} = \frac{32\eta}{\pi e^2 n^2 w^2}. \tag{3.40}$$

This is precisely the hydrodynamic result given in Eq.(1.1).

Now we proceed to solve for the 2D potential distribution and current flow in the hydrodynamic regime $\gamma \gg v/w$. We transform the semicircle solution Eq.(3.38) to Fourier domain:

$$g(k) = \int_{-\frac{w}{2}}^{\frac{w}{2}} g(x) e^{-ikx}\, \mathrm{d}x = \frac{\pi w a}{2} \frac{J_1(|kw/2|)}{|kw/2|}, \tag{3.41}$$

where J_1 is the Bessel Function. The solution of the 1D problem can be used to obtain the 2D flow by using the same procedure as the one employed to obtain the density distribution, Eq.(3.31). Using the values $\tilde{G}_{cs}$ and $\tilde{G}_{ss}$ given in Eq.(3.13), and approximating $D_{ss}^{-1} \approx |k_x| v^2/\gamma$, the $|c\rangle$ and $|s\rangle$ components of the flow are given by

$$f(k_x, k_y) = \frac{4\pi a}{v^2} J_1(|k_x w/2|) \begin{pmatrix} \frac{-k_x k_y}{k^4} \\ \frac{k_x^2}{k^4} \end{pmatrix}, \tag{3.42}$$

where the two entries represent the x and y momentum components, respectively. In the equation above, the μ term does not contribute. The next step is to perform Fourier transform to obtain the real-space flow distribution

$$f(x, y) = \int \frac{\mathrm{d}k_x}{2\pi} \frac{\mathrm{d}k_y}{2\pi} f(k_x, k_y) e^{ik_x x + ik_y y}. \tag{3.43}$$

After the k_y integral is calculated by the residue method, we have

$$\begin{aligned} f(x, y) &= \int \frac{\mathrm{d}k_x}{2\pi} \frac{\pi a e^{ik_x x - |k_x y|}}{v^2} J_1(|k_x w/2|) \begin{pmatrix} -iy \\ \frac{1+|k_x y|}{|k_x|} \end{pmatrix} \\ &= \mathrm{Re} \int_0^\infty \mathrm{d}k_x \frac{a e^{ik_x x - |k_x y|}}{v^2} J_1(|k_x w/2|) \begin{pmatrix} -iy \\ \frac{1+|k_x y|}{|k_x|} \end{pmatrix}, \end{aligned} \tag{3.44}$$

The k_x integral can be evaluated using the identity

$$\int_0^\infty e^{-\alpha x} J_\nu(\beta x) = \frac{\beta^{-\nu}(\sqrt{\alpha^2+\beta^2}-\alpha)^\nu}{\sqrt{\alpha^2+\beta^2}}. \tag{3.45}$$

This gives the flow velocity components:

$$\begin{aligned} f_x &= -\frac{2a}{wv^2}\,\mathrm{Im}\left(y\frac{|y|-ix}{Z}\right), \\ f_y &= \frac{2a}{wv^2}\,\mathrm{Re}\left(Z-|y|\frac{|y|-ix}{Z}\right), \\ Z &= \sqrt{(w/2)^2+(|y|-ix)^2}. \end{aligned} \tag{3.46}$$

The resulting flow is shown in Fig.2-2. Using Eq.(3.31) we can compute the density distribution:

$$f_0(x,y) = \frac{\operatorname{sgn} y}{\sqrt{2}v}\left(\frac{2av^2}{\gamma w}\,\mathrm{Re}\left(1-\frac{|y|-ix}{Z}\right)-\mu\right). \tag{3.47}$$

The value of μ can be alternatively determined by f_0 being continuous at the slit, giving $\mu = 2v^2a/\gamma w$, which agrees with the previous result.

3.6 Numerical Analysis

In this section, we describe the details of numerical analysis to the central equation Eq.(3.28).

3.6.1 Discretization

To facilitate numerical analysis, we put our 2D problem on a cylinder, choosing a large enough cylinder circumference L to provide a good approximation to the 2D problem. Closing the x axis into a circle does not impact in any way the 2D $\rightarrow$ 1D

reduction, which yields an integral equation defined in the domain $[-\frac{1}{2}L, \frac{1}{2}L]$:

$$\alpha(x)g(x) + \int_{-L/2}^{L/2} dx' \tilde{D}_{ss}^{-1}(x-x')g(x')dx' = \mu, \tag{3.48}$$
$$\tilde{D}_{ss}^{-1}(x-x') = \sum_{m=-\infty}^{\infty} D_{ss}^{-1}(x-x'-mL),$$

with periodic boundary conditions, $g(x \pm L) = g(x)$. It may seem that the problem defined by Eq.(3.48) is identical to that in Eq.(3.33), since any function $g(x)$ satisfying Eq.(3.48), after being continued periodically outside the domain $[-\frac{1}{2}L, \frac{1}{2}L]$, satisfies also Eq.(3.33). We note, however, that such a procedure generates functions which are nonzero not only in the slit interval $[-\frac{w}{2}, \frac{w}{2}]$ $(w < L)$ but also in the intervals $[Lm - \frac{w}{2}, Lm + \frac{w}{2}]$ where the solution of the original problem, Eq.(3.33), must vanish in the limit $b \to \infty$. Physically, this is equivalent to replacing one slit with an infinite array of slits of width w each, and periodicity L. The behavior near one slit will not be affected by other slits so long as $L \gg w$. In our numerical study, taking L equal few times w was found sufficient to provide a reasonably good approximation.

To handle the L-periodic boundary conditions, we write Eq.(3.48) in momentum space, with momentum taking discrete values

$$k = \frac{2\pi n}{L}, \tag{3.49}$$

where n is an integer. We transform Eq.(3.48) by inserting a resolution of identity $\frac{1}{L}\sum_k |k\rangle\langle k| = 1$, and using $\langle x|k\rangle = \exp(ikx)$, $D|k_x\rangle = D_{ss}(k_x)|k_x\rangle$, and $\langle k|g(x)\rangle = g_k$, where

$$g_k = \int_{-L/2}^{L/2} dx e^{-ikx} g(x). \tag{3.50}$$

Finally, we obtain:

$$\sum_{k_1} \alpha_{k-k_1} g_{k_1} + D_{ss}^{-1}(k) g_k = \mu L \delta_{k,0}, \tag{3.51}$$

where $\alpha_k = b(\delta_{k,0} - \frac{w}{L}\mathrm{sinc}(kw/2))$. In numerical calculation, the values n in Eq.(3.49) are limited by $-\frac{1}{2}N \le n < \frac{1}{2}N$, where N is a suitably chosen large number. This

corresponds to discretizing functions $f(x)$ in position space by using an N-point mesh $x_i = \frac{iL}{N}$, $i = -\frac{N}{2}, -\frac{N}{2}+1, ..., \frac{N}{2}-1$ in the interval $[-\frac{1}{2}L, \frac{1}{2}L]$.

3.6.2 Numerical Results

We solve Eq.(3.51) numerically to obtain current distributions pictured in Fig.3-1. This was done by first finding the distribution f_k in momentum space, and then Fourier-transforming to position space. We used $L = 3w$, and a large value $b = 10^5 v$ to ensure that current vanishes outside the interval $|x| < \frac{w}{2}$. When transforming back to position representation, a Fourier space filter

$$g_k \to g_k \operatorname{sinc} \frac{kL}{2N}$$

was used to smooth out the Gibbs phenomenon near the points $x = \pm\frac{w}{2}$ where current distribution drops abruptly to zero.

In the plots the value μ was chosen such that the net current is normalized to unity. The resulting current distribution evolves in an interesting way upon γ increasing: the distribution is a flat step at small γ, as expected in the ballistic case, and then gradually bulges forming a peak at $x = 0$ and gradually dropping to zero near $x = \pm\frac{w}{2}$. In the extreme hydrodynamic limit $\gamma \gg v/w$, it evolves into a semicircle, which coincides with the previous analytic results.

Using the solution g_k, resistance R can be calculated from Eq.(3.32), giving the conductance $G = 1/R$ shown in Fig.3-3 and Fig.3-4.

The dependence R vs. γ shows several interesting features, some expected and some unexpected.

First, on general grounds, we expect that the dependence on γ is controlled solely by the ratio w/l_{ee}. For large $b = 10^6 v$, the conductance plots G vs. γ, obtained for different slit widths w, collapse on one curve when rescaled to G/w vs. γw. This 'universality' confirms that the only relevant parameter in the problem is the ratio w/l_{ee}. This scaling stops working already for not very large b, as illustrated in Fig.3-4. The breakdown of scaling is not alarming, since physically meaningful results are

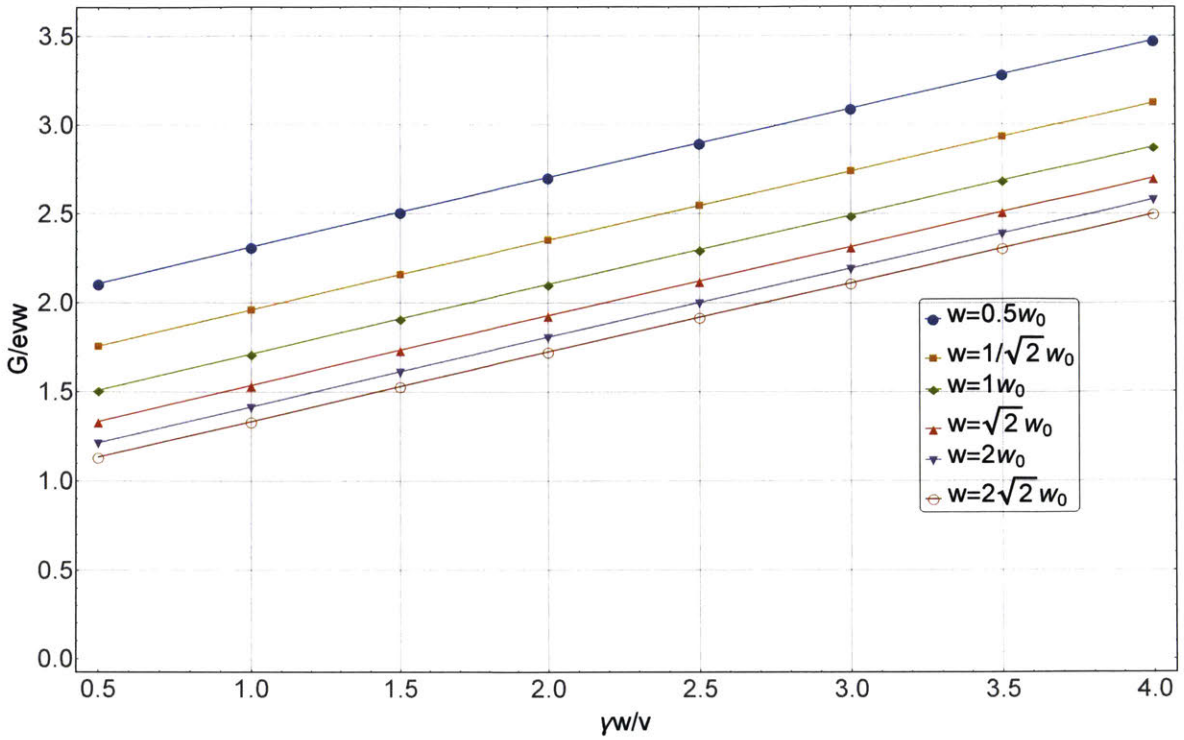

Figure 3-4: Conductance per width vs. γw. Plots are obtained at $w_0 = \frac{1}{30}L$, $b = 50v$, with the number of sampling points within the slit of about 160. Unlike Fig.3-3, here different curves do not collapse on one curve, indicating that the universality fails for small b.

expected only in the limit $b \to \infty$. Interestingly, however, the dependence G/w vs. γw is well fitted by a perfectly straight line both for b large and not-too-large. The linear dependence G vs. γ, along with the scaling, indicate that the conductance at the crossover is described by the addition formula

Second, quite remarkably, inverting this quantity and plotting $1/(Rw)$ vs. γw we find *a nearly perfect straight line* with a positive offset at $\gamma = 0$, see Fig.3-3b. The straight line, which is identical for all w values, is described by $\rho_*/(Rw) = a_1 + a_2\gamma w$. This dependence translates into a simple addition rule for conductance,

$$G = G_{\text{ball}} + G_{\text{vis}}. \tag{3.52}$$

The term G_{ball} describes a γ-independent ballistic contribution that scales linearly with w, whereas G_{vis} describes a viscous contribution proportional to γ that scales as w^2. By comparing to the two analytic limits, the two terms yield values $a_1 = 2/\pi$

and $a_2 = \pi/8$, respectively. This is in good agreement with the values $a_1 = 0.694$, $a_2 = 0.378$ obtained from a best fit to the data in Fig.3-3b.

The additive behavior of conductance at the ballistic-to-viscous crossover comes as a surprise and, to the best of our knowledge, is not anticipated on simple grounds. This is in a stark departure from the Matthiessen's rule that mandates an additive behavior for resistivity in the presence of different scattering mechanisms, as observed in many solids[33]. This rule is of course not valid if the factors affecting transport depend on each other, because individual scattering probabilities cannot be summed unless they are mutually independent. This is precisely the case for momentum-conserving ee collisions that do not by themselves result in momentum loss, but can impact momentum relaxation due to other scattering mechanisms. Furthermore, the addition rule for conductance, Eq.(3.52), describes a striking "anti-Matthiessen" behavior: rather than being suppressed by collisions, conductance exceeds the collisionless value.

3.7 Including Ohmic Effects

In this section, we will extend our formalism to incorporate ohmic effects, i.e. momentum-nonconserving scattering due to disorder, phonons, etc. This will help us to understand the impact of ohmic effects on the ballistic regime, the hydrodynamic regime, and on the crossover between them.

In contrast to electron-electron scattering where both particle number and momentum are conserved (the angular harmonics $m = 0, \pm 1$), ohmic scattering only conserves particle number (the $m = 0$ harmonics). We therefore modify the bulk collision term Eq.(3.3) as follows:

$$I_{ee}(f) = -\gamma_{\text{viscous}}(1 - P_0 - P_\pm)f - \gamma_{\text{ohmic}}(1 - P_0)f. \tag{3.53}$$

Here γ_{viscous} and γ_{ohmic} denote the rates of the two scattering mechanisms respectively. For convenience, we define $\gamma = \gamma_{\text{viscous}} + \gamma_{\text{ohmic}}$ to be the total scattering rate, and $\rho = \gamma_{\text{ohmic}}/\gamma$ to be the fraction of ohmic scattering.

To solve this problem, we return to Eq.(3.9):

$$(1 + \tilde{G}\hat{\alpha}) \left| \tilde{f} \right\rangle = \left| f^{(0)} \right\rangle, \tag{3.54}$$

where again $\tilde{f} = f^{(0)} + P\delta f$, and $f^{(0)}$ describes the flow in free space in absence of the slit. In presence of momentum scattering, $f^{(0)} = |s\rangle - \sqrt{2}\gamma_{\text{ohmic}} y/v \, |0\rangle$ is a uniform flow in the y direction together with a potential gradient.

The Green's function can be worked out using the Lippmann-Schwinger methods, yielding the counterpart of Eq.(3.12):

$$\tilde{G} = \frac{1}{1 - SV} \gamma^{-1} S, \tag{3.55}$$

where $V = P_0 + (1 - \rho)P_\pm$, and S is defined by Eq.(3.10).

It is convenient to write the above result in the $|0\rangle$, $|c\rangle$, $|s\rangle$ basis, which gives

$$\tilde{G} = \begin{pmatrix} \frac{2\rho+R_-}{\gamma\kappa^2} & \frac{-i\sqrt{2}\kappa_1}{\gamma\kappa^2} & \frac{-i\sqrt{2}\kappa_2}{\gamma\kappa^2} \\ \frac{-i\sqrt{2}\kappa_1}{\gamma\kappa^2} & \frac{2\kappa_2^2}{\gamma\kappa^2(2\rho+R_-)} & \frac{-2\kappa_1\kappa_2}{\gamma\kappa^2(2\rho+R_-)} \\ \frac{-i\sqrt{2}\kappa_2}{\gamma\kappa^2} & \frac{-2\kappa_1\kappa_2}{\gamma\kappa^2(2\rho+R_-)} & \frac{2\kappa_1^2}{\gamma\kappa^2(2\rho+R_-)} \end{pmatrix}, \tag{3.56}$$

where as before $R_-(\kappa) = \sqrt{\kappa^2+1} - 1$, $\kappa_{1,2} = \frac{v}{\gamma}k_{1,2}$, $\kappa = \sqrt{\kappa_1^2+\kappa_2^2}$.

The next step is to project Eq.(3.54) onto $y = 0$ line. Making use of the $x \to -x, y \to -y$ inversion symmetry, we can write $\tilde{f}(\theta, x) = g(x)\sqrt{2}\sin\theta$, and g satisfies equation

$$(1 + D_{ss}\alpha)\,|g\rangle = \left|g^{(0)}\right\rangle. \tag{3.57}$$

The operator $D_{ss}(k_1) = \int \frac{\mathrm{d}k_2}{2\pi}\tilde{G}_{ss}(k_1, k_2)$ is :

$$D_{ss}(\kappa) = \frac{\kappa}{4(1-\rho)\rho} \times \left[\frac{\kappa(2\rho-1)\left(1 - \frac{2}{\pi}\tan^{-1}\frac{2\rho-1}{\sqrt{\kappa^2+4(1-\rho)\rho}}\right)}{\sqrt{\kappa^2+4(1-\rho)\rho}} + \frac{2\cot^{-1}\kappa}{\pi} - (2\rho-1)\mathrm{sgn}\kappa \right], \tag{3.58}$$

where $\kappa = kv/\gamma$.

As a sanity check, if we keep $\kappa > 0$ and take the $\rho \to 0$ limit of Eq.(3.58), we indeed recover the viscous version Eq.(3.26). However, the $\kappa = 0$ case is more subtle because Eq.(3.58) predicts $D_{ss}(0) = 0$ for any $\rho > 0$, whereas Eq.(3.26) says $D_{ss}(0) = \infty$. This discrepancy is due to the fact that $(\kappa, \rho) = (0, 0)$ is a branch point of D_{ss}, and if we expand around $\rho = 0$, all terms have poles at $\kappa = 0$. Therefore even if there are no ohmic effects, we should still include a infinitesimal ρ which acts as a regulator such that $D_{ss}(0) = 0$.

The above discussion not only required the introduction of the μ-term in the central equation Eq.(3.28), but also required it to be *infinite*. To circumvent this problem, we can discard the $k = 0$ component of the central equation, and replace it

by the current normalization condition $g_{k=0} = g^{(0)}_{k=0} = 1$. Solving the central equation with such a modification will produce the correct g_k that describes the flow within the slit.

However, because previously we could conveniently interpret μ as the potential drop across the slit, it would be helpful to find the equivalent of such a quantity here. We note in that regard that when the flow in the bulk was calculated, e.g. in Eq.(3.31), the quantity μ always appeared in the combination $D_{ss}^{-1}(k)g_k - 2\pi\mu\delta(k)$, and it was the $k = 0$ value of it that determined the total potential drop. Motivated by this observation, we define the new μ' to be the above combination. However, since it is the difference between two divergent quantities, a prescription for evaluating it must be specified. Using the central equation Eq.(3.28) we get

$$2\pi\mu'\delta(0) = \int \frac{dk'}{2\pi}\alpha_{k'}g_{k'}, \tag{3.59}$$

where in numerical calculations $2\pi\delta(0)$ will be replaced by the system size L.

To calculate the potential in the bulk, we write down the modified version of Eq.(3.31):

$$\delta f_0(\mathbf{x}) = \frac{\operatorname{sgn} y}{\sqrt{2}v}\int \frac{dk_1}{2\pi}e^{ik_1x-|k_1y|}\left(D'^{-1}_{ss}(k_1)g_{k_1} - 2\pi\mu'\delta(k_1)\right), \tag{3.60}$$

where D'^{-1}_{ss} agrees with D^{-1}_{ss} at $k \neq 0$ and vanishes at $k = 0$. Here δf_0 captures the potential drop due to the slit, from which the bulk resistivity effect is subtracted.

Using this approach, we can calculate the flow distribution at the slit and the potential distribution in the bulk. The results for the crossover between the hydrodynamic and ohmic regimes are shown in Fig.3-5 (a). We observe that as γ_{ohmic} increases, the flow distribution evolves from a semicircle to a double-spike distribution. Interestingly, the transition to the ohmic regime happens when $\gamma_{\text{ohmic}}w/v \sim 1$, regardless of the ee collision mean free path value. This crossover value $\gamma_{\text{ohmic}} \sim v/w$ corresponds to the ohmic momentum relaxation mean free path being comparable to the slit width.

The ballistic-to-ohmic crossover, shown in Fig.3-5 (b), features a similar behav-

ior: the current profile in the slit evolves from a flat distribution to a double-spike distribution, with the same crossover value for the ohmic rate, $\gamma_{\text{ohmic}} \sim v/w$. The potential distribution for the ohmic regime, shown in Fig.3-6, has the shape similar to the ballistic result in Fig.3-2(a).

We used the method described above to calculate potential drop across the slit and determined resistance dependence on the ohmic rate γ_{ohmic} and the electron-electron scattering rate γ_{viscous}. We found that in the not-too-extreme ohmic regime where $\gamma_{\text{ohmic}} \sim v/w$, the total resistance R decreases as γ_{viscous} increases. This means that the hydrodynamic conduction enhancement survives in the presence of weak phonon scattering and disorder scattering. Somewhat unexpectedly, the total resistance could be fitted pretty accurately by a series resistance formula

$$R = \tilde{R}_{\text{ohmic}} + \frac{1}{\tilde{G}_{\text{ballistic}} + \tilde{G}_{\text{viscous}}}, \tag{3.61}$$

which can be viewed as an "ohmic generalization" of the conductance addition formula Eq.(1.3). We use tilde to indicate that the quantities are fitting parameters that in the limit $\gamma_{\text{ohmic}} \to 0$ turn into the quantities introduced earlier. Here the parameters $\tilde{R}_{\text{ohmic}}$ and $\tilde{G}_{\text{ballistic}}$ are independent of γ_{viscous} and $\tilde{G}_{\text{viscous}}$ is proportional to γ_{viscous}. However, all of these quantities depend on γ_{ohmic}: As γ_{ohmic} increases, $\tilde{R}_{\text{ohmic}}$ increases whereas $\tilde{G}_{\text{ballistic}}$ and $\tilde{G}_{\text{viscous}}$ decrease, which suggests that the interaction-induced conduction enhancement is suppressed by strong ohmic scattering, in which case we recover the conventional ohmic regime.

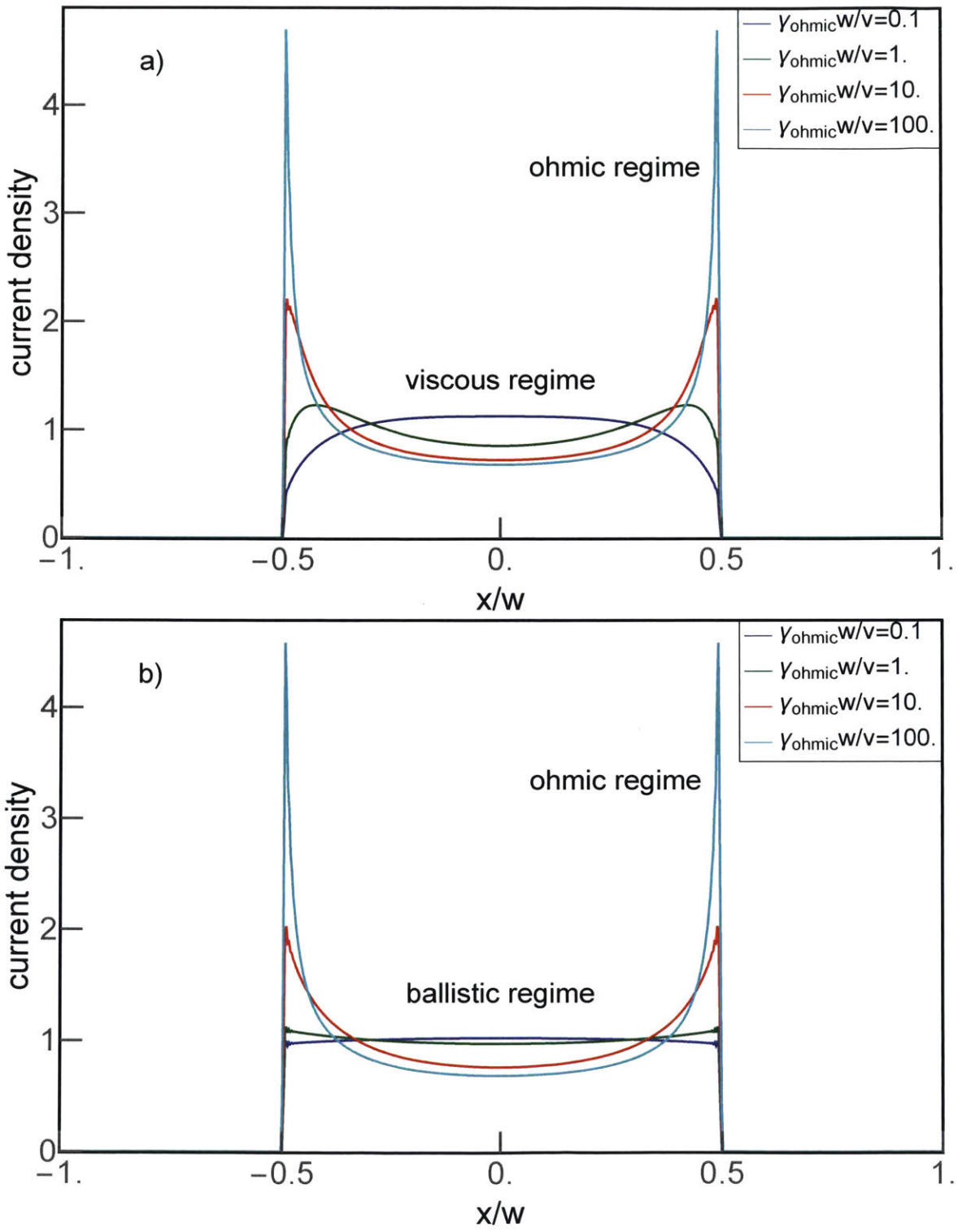

Figure 3-5: Current distributions in the slit for different ohmic scattering rates, illustrating the hydrodynamic-to-ohmic (a) and ballistic-to-ohmic (b) crossovers. The total current is normalized to 1. When γ_{ohmic} is small, the distributions are in the viscous regime and ballistic regime, respectively. As γ_{ohmic} increases, they evolve to the ohmic double-spike distribution. Parameters used: γ_{viscous} =(a) $50v/w$, (b) $0.5v/w$; other parameter values are the same as Fig.3-1

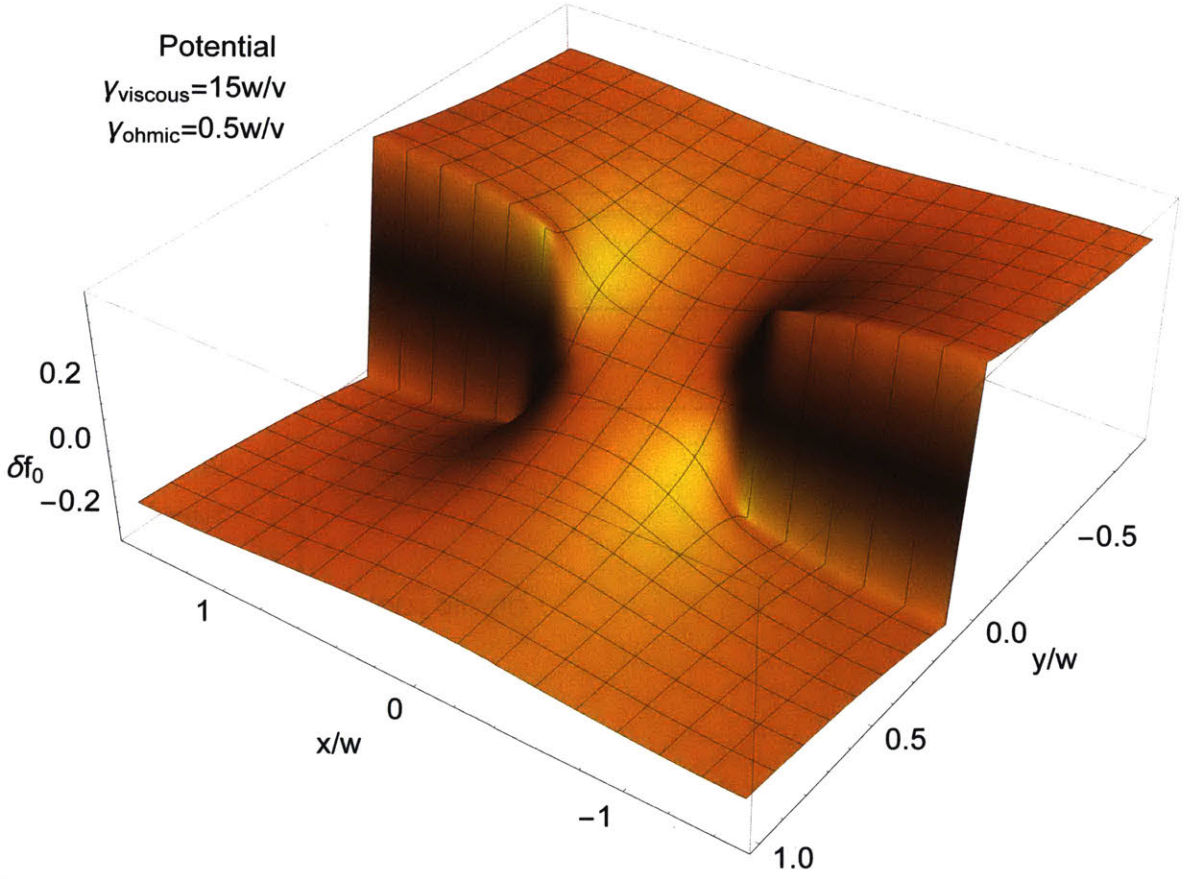

Figure 3-6: Potential distribution induced by current through the slit in the ohmic regime. The bulk resistivity contribution, linear in y, has been subtracted. Parameters: $\gamma_{\text{viscous}} = 15v/w$, $\gamma_{\text{ohmic}} = 0.5v/w$.

Chapter 4

Conclusion and Outlook

In this thesis, we have studied signatures of hydrodynamic transport in an electron system. The main finding of this work is that in the hydrodynamic regime strongly interacting electrons "cooperate": by exchanging momenta through two-body collisions they move more easily than in the absence of collisions. In a sense, they achieve collectively what they cannot accomplish individualy, overcoming the ballistic conduction limit. Starting with this motivation, we went through the following steps to substantiate this picture:

In chapter 2, we compared ballistic transport and hydrodynamic transport in a slit geometry. We reviewed the theory of ballistic transport and derived the Landauer-Sharvin conductance. We used the Navier-Stokes equation to model the hydrodynamic regime, and calculated the potential distribution, flow distribution and the conductance. We demonstrated that there are several interesting signatures for hydrodynamic transport, such as superballistic conduction and non-monotonic potential distribution.

In chapter 3, we used Boltzmann equation to establish a theory covering the crossover from the ballistic regime and hydrodynamic regime. By using a simple model for electron-electron collisions, the problem was made analytically tractable. We calculated the Green's function of the system, and along the way we obtained the collective modes and the viscosity. The problem was further simplified by projecting the two-dimensional equation onto the slit line. Through numerical analysis of the

projected equation, we obtained the conductance as a function of the electron-electron scattering rate. Surprisingly, the result was a simple linear dependence within the (very high) numerical precision of our method. This linear dependence translates into the addition formula that the net conductance, which is given by a sum of the ballistic conductance and the hydrodynamic conductance. We also explored the transition to ohmic flow by introducing ohmic scattering into the Boltzmann equation.

Thinking about the future, there are several aspects that seem interesting to explore further. First, our numerical calculation gives a strong evidence for the addition formula to be exact, so it would be really interesting to understand analytically how the addition formula arises. This is far from being clear at the moment, however one could explore approaches that use holographic duality to map the problem to some gravitational system, in which the addition formula may hopefully become manifest. Second, our preliminary results suggest that the simple collision integral model used in this work may be oversimplified. For example, it fails to acknowledge the fact that in two-dimensions the odd harmonics of the perturbed momentum distribution near the Fermi surface relax slower than the even harmonics, due to phase space constraints. A better understanding of these aspects of the collision operator may add some interesting features to the hydrodynamic theory, in particular new collective modes. Third, we have assumed the system to be in the Fermi liquid state. In the future, it would also be interesting to explore the hydrodynamics in the Dirac fluid phase, where the system is undoped and the Fermi level is aligned with the Dirac point. In this case the emergent Lorentz symmetry may play a important role in the theory.

Bibliography

[1] R. Landauer, *IBM Journal of Research and Development*, **1**: 223-231 (1957).

[2] Yu. V. Sharvin, *Sov. Phys. JETP* **21**, 655 (1965).

[3] B. J. van Wees, H. van Houten, C. W. J. Beenakker, J. G. Williamson, L. P. Kouwenhoven, D. van der Marel, and C. T. Foxon, Phys. Rev. Lett. **60**, 848 (1988).

[4] D. A. Wharam, T. J. Thornton, R. Newbury, M. Pepper, H. Ahmed, J. E. F. Frost, D. G. Hasko, D. C. Peacock, D. A. Ritchie and G. A. C. Joneset, J. Phys. C **21**, L209 (1988).

[5] D. L. Maslov and M. Stone, Phys. Rev. B**52**, R5539 (1995).

[6] H. van Houten and C. W. J. Beenakker, Physics Today **49** (7): 22-27 (1996).

[7] R. N. Gurzhi, *Usp. Fiz. Nauk* **94**, 689 [Engl. transl.: *Sov. Phys. Usp.* **11**, 255 (1968)].

[8] E. M. Lifshitz and L. P. Pitaevskii, *Physical Kinetics* (Pergamon Press 1981).

[9] R. Jaggi, *J. Appl. Phys.* **69**, 816-820 (1991).

[10] K. Damle and S. Sachdev, *Phys. Rev. B* **56**, 8714 (1997).

[11] M. Müller, J. Schmalian, and L. Fritz, *Phys. Rev. Lett.* **103** 025301 (2009).

[12] M. Mendoza, H. J. Herrmann, and S. Succi *Phys. Rev. Let.* **106**, 156601 (2011).

[13] N. Sai, M. Zwolak, G. Vignale, and M. Di Ventra, *Phys. Rev. Lett.* **94**, 186810 (2005).

[14] D. Roy, G. Vignale, and M. Di Ventra, *Phys. Rev. B* **83**, 075428 (2011).

[15] A. V. Andreev, S. A. Kivelson, and B. Spivak, *Phys. Rev. Lett.* **106**, 256804 (2011).

[16] D. Forcella, J. Zaanen, D. Valentinis, and D. van der Marel, *Phys. Rev. B* **90**, 035143 (2014).

[17] A. Tomadin, G. Vignale, and M. Polini, *Phys. Rev. Lett.* **113**, 235901 (2014).

[18] D. E. Sheehy and J. Schmalian, *Phys. Rev. Lett.* **99**, 226803 (2007).

[19] L. Fritz, J. Schmalian, M. Müller, and S. Sachdev, *Phys. Rev. B,* **78** 085416 (2008).

[20] B. N. Narozhny, I. V. Gornyi, M. Titov, M. Schütt, and A. D. Mirlin, *Phys. Rev. B* **91**, 035414 (2015).

[21] A. Principi, G. Vignale, M. Carrega, and M. Polini, Phys. Rev. B **93**, 125410 (2016).

[22] A. Cortijo, Y. Ferreirós, K. Landsteiner, and M. A. H. Vozmediano, Phys. Rev. Lett. **115**, 177202 (2015).

[23] A. Lucas, J. Crossno, K. C. Fong, P. Kim, and S. Sachdev, Phys. Rev. B 93 (7), 075426 (2016).

[24] M. J. M. de Jong, and L. W. Molenkamp, *Phys. Rev. B* **51**, 13389-13402 (1985).

[25] D. A. Bandurin, I. Torre, R. Krishna Kumar, M. Ben Shalom, A. Tomadin, A. Principi, G. H. Auton, E. Khestanova, K. S. Novoselov, I. V. Grigorieva, L. A. Ponomarenko, A. K. Geim, and M. Polini, *Science* **351**, 1055-1058 (2016).

[26] J. Crossno, J. K. Shi, K. Wang, X. Liu, A. Harzheim, A. Lucas, S. Sachdev, P. Kim, T. Taniguchi, K. Watanabe, T. A. Ohki, and K. C. Fong, Science **351** (6277), 1058-1061 (2016).

[27] P. J. W. Moll, P. Kushwaha, N. Nandi, B. Schmidt, and A. P. Mackenzie, Science **351** (6277) 1061-1064 (2016).

[28] K. E. Nagaev and O. S. Ayvazyan, *Phys. Rev. Lett.***101**, 216807 (2008).

[29] R. S. Marvin, J. Res. Nat. Bur. Stand. (U.S.) **75**A, (Phys. and Chem.), No.6, 535-540 (1971).

[30] I. B. Levinson, *Sov. Phys. JETP* **46** 165-172 (1977).

[31] G. Falkovich and L. Levitov, Phys. Rev. Lett. **119**, 066601 (2017).

[32] L. Levitov and G. Falkovich, Nature Phys. **12**, 672-676 (2016).

[33] F. J. Blatt, "Matthiessen's rule" (McGraw-Hill, 2014).

[34] Haoyu Guo, Ekin Ilseven, Gregory Falkovich, and Leonid S. Levitov, Proceedings of the National Academy of Science, vol. 114 no. 12, 3068-3073 (2017).

[35] R. Krishna Kumar *et al*, Nature Physics. **13** 1182-1185 (2017).

[36] James Jeans, *An Introduction to the Kinetic Theory of Gases,* Cambridge Science Classics (1982).

[37] Dmitri K. Efetov and Philip Kim Phys. Rev. Lett. **105**, 256805 (2010).